

**Editor Decision: Reconsider after minor revisions (Editor review)** (05 May 2015) by Xiaobin Xu

Comments to the Author:

Dear authors,

Please study carefully the referee report #2, address the remaining issues and make technical changes as suggested.

Sincerely,  
Xiaobin Xu

Dear Editor,

We have addressed the minor issues raised by the referee, but do not agree with the two main suggestions for the reasons detailed below. Regarding the major concern of the referee on our efficiency metric, we want to stress that the metric (which weights source region contributions by their own emissions) and the associated results (Fig. 7) and discussion are neither flawed nor vaguely presented. As we now explain in the manuscript, the efficiency metric is proportional to the sensitivity coefficient ( $\Delta BC_{concentration}/\Delta emissions$ , or  $\Delta BC_{deposition}/\Delta emissions$ ), which has been used in other source-receptor studies (e.g., Shindell et al., 2008; Wang et al., 2014; references are provided in the revised manuscript.). Also, it complements the relative contribution metric used in the paper. However, as a compromise, we have removed the local emissions (HTP) efficiency from the figure, as it could potentially cause misinterpretation of our main results.

Thanks,

Hailong Wang (on behalf of all authors)

### **Referee Report #2**

Title: Quantifying sources, deposition, transport and radiative forcing of black carbon over the Himalayas and Tibetan Plateau

Authors: Rudong Zhang, Hailong Wang, Yun Qian, Philip J. Rasch, Richard C. Easter, Po-Lun Ma, Balwinder Singh, Jianping Huang, and Qiang Fu

General Comment

Thanks for the detailed responses and revisions in reply to both my comments and to those from the other referee. However, after reviewing the author response to my

comment about efficacy, I strongly recommend the discussion of efficacy be removed entirely before the manuscript is published. The authors themselves state (line 251): “This metric [efficiency] is of more interest to policy makers for the purpose of mitigation action, which is not the focus of this study but is worth mentioning.” This single phrase should be enough to suggest the discussion is not contributing to the basic findings of the study, but I provide a much more extensive critique below.

#### Specific Comment

Line 94-5: change “slow down the climate change” to “slow down present-day climate change”

[Done as suggested.](#)

Section 4.1 and 4.3: I agree that including all the source region graphics from figure S3 in the main text would be unnecessary, but please add cross-referencing to figure S3 throughout these two sections since figures 4 and 6 do not have the information about other regions (like RBU) you are often alluding to. Figure S3 seems really useful to repeatedly bring to the attention of the reader.

[Done as suggested.](#)

Figure 6: please make this figure just like was done for figure 7! Figure 6 is not nearly as clear to me as figure 7. A category for “all other source regions” (black in figure 6) could still be included, and the relative contributions of FF and BB could be easily be noted in text within the figure. This would make the message much clearer and draw out the results from figure 6.

[We disagree with this suggestion. We would argue that the bar chart \(with color-coded elements\) is more effective and straightforward than using the color scheme alone \(like in Figure 7\) for comparing the magnitudes between different contributors/sources and showing seasonal variations of relative contributions by individual sources. It also facilitates the comparison of contributions between burden and deposition by placing them side-by-side. Moreover, the colors make it easy to compare contributions of individual regions to the different receptors across the various panels.](#)

Section 4.4 and Efficiency: Thanks for the explanation, but I still do not think this section or figure 7 are relevant to the paper. It comes down to a metric that can be 1. Easily misinterpreted, and 2. Misinterprets the results. As pointed out by the authors in the response to my original comment, efficiency is a relative metric suggesting the importance of relative changes to emissions from source regions to HTP and sub-regions. Figure 7 shows that HTP is the most important contributor to its own BC. This is not surprising given essentially common knowledge about aerosol lifetimes. The real message is in figure 6 – what regions determine absolute contributions to BC burden and deposition over HTP.

Figure 7 waters down the enormous impact (burden and deposition) of SAS and EAS on HTP and, to varying degrees, on HTP sub-regions, as shown in figure 6. This watering down is evident in the author response: “In other words, the efficiency of local emissions in affecting HTP BC is very high (Figure 8), which means that the impact of per-unit-mass (or equal-magnitude) perturbation in emissions on BC over HTP is much stronger if the perturbation occurs within HTP than in any other source regions including SAS and EAS.” The key words are that the authors are viewing the impact of a perturbation in emissions within HTP. My original comment was whether that was relevant to HTP when I said “HTP has practically no emissions and I do not see how anyone could practically expect HTP to develop major emission sources.” In other words, what could happen in HTP that would perturb the emissions in any way? Are power plants expected to be built there? Are fires expected to increase? Population?

Look at my point another way using your own numbers, roughly shown in the table below. Numbers I label “Efficiency” are values under “Figure 6a (approx)” divided by “ $E_i/E_{total}$  (fraction)” under “Combine Fig 1 and S1”. The conclusion that could be read is that emissions controls/mitigation in SAS and EAS is not as needed as making sure HTP keeps emissions low since HTP has a higher efficiency (191 vs 19 for SAS and 2.1 for EAS). The higher efficiency is a result of dividing a comparable contribution (0.11 for HTP, vs 0.17 for EAS, vs 0.49 for SAS, estimated from figure 6a) by a very small number – HTP total emissions are 143x less than EAS and 45x less than SAS. Altogether this obfuscates the real problem: absolute contributions from SAS and EAS. If SAS and EAS stopped emitted BC, HTP burden would drop precipitously.

I strongly recommend dropping the discussion of efficiency in this manuscript, and dropping the equation and discussion for efficiency in Section 2.2. This is better left to a dedicated study that talks more deeply about what this actually means for policy makers.

Figure 1 (direct)

BM-BB (Tg/yr)	BF-BB (Tg/yr)	FF (Tg/yr)	total (Tg/yr)
2.61	1.76	3.41	7.78

Table S1 (direct)

	BM-BB (%)	BF-BB (%)	FF (%)
SAS	0.65	5.56	2.58
EAS	0.64	5.7	15.3
HTP	0	0.08	0.09

Combine Fig 1 and S1

	BM-BB (Tg/yr)	BF-BB (Tg/yr)	FF (Tg/yr)	total (Tg/yr)	$E_i/E_{total}$ (fraction)
SAS	0.0170	0.0979	0.0880	0.2028	0.0261
EAS	0.0167	0.1003	0.5217	0.6388	0.0821
HTP	0.0000	0.0014	0.0031	0.0045	0.0006

Figure 6a (approx)

$C_i$  to HTP (fraction)

SAS 0.49  
EAS 0.17  
HTP 0.11

Efficiency (from Fig 6, Fig 1, Table S1)

SAS 18.80  
EAS 2.07  
HTP 191.15

We appreciate the referee's effort in illustrating the point here, and we agree that the reason for the much higher efficiency of the HTP local emissions is quite obvious. With the significant contributions but very little emissions, the local sources are very effective in contributing to BC in the HTP. Although there is not much that can be done to HTP local emissions for any mitigation actions, the quantitative efficiencies indicate that a small uncertainty in local emissions could largely impact the magnitude of local contributions to BC over the HTP. This efficiency metric is of more interest to policy makers, but it is also informative to researchers who prepare emission inventories for models and are interested in knowing the quantitative impact of uncertainties in regional emissions. We disagree with the referee that the efficiency is irrelevant to the focus of this study. However, we agree that the magnitude of efficiency for HTP emissions is relatively large and could potentially cause misinterpretations of the main results of this study. To address the referee's main concern, we have removed the HTP (local sources) efficiency from Figure 7, so the emphasis is now on the major source regions such as SAS and EAS.

# **Quantifying sources, transport, deposition and radiative forcing of black carbon over the Himalayas and Tibetan Plateau**

Rudong Zhang<sup>1, 2, 3</sup>, Hailong Wang<sup>2</sup>, Yun Qian<sup>2</sup>, Philip J. Rasch<sup>2</sup>, Richard C. Easter<sup>2</sup>, Po-Lun Ma<sup>2</sup>, Balwinder Singh<sup>2</sup>, Jianping Huang<sup>1</sup>, and Qiang Fu<sup>1, 3</sup>

<sup>1</sup> Key Laboratory for Semi-Arid Climate Change of the Ministry of Education, College of Atmospheric Sciences, Lanzhou University, Lanzhou 730000, Gansu, China.

<sup>2</sup> Atmospheric Sciences and Global Change Division, Pacific Northwest National Laboratory (PNNL), Richland, WA 99352, USA.

<sup>3</sup> Department of Atmospheric Sciences, Box 351640, University of Washington, Seattle, WA 98195, USA.

Manuscript for submission to *Atmospheric Chemistry and Physics*

Correspondence to: Hailong.Wang@pnnl.gov

## Abstract

1  
2 Black carbon (BC) particles over the Himalayas and Tibetan Plateau (HTP), both airborne and  
3 those deposited on snow, have been shown to affect snowmelt and glacier retreat. Since BC over  
4 the HTP may originate from a variety of geographical regions and emission sectors, it is essential  
5 to quantify the source-receptor relationships of BC in order to understand the contributions of  
6 natural and anthropogenic emissions and provide guidance for potential mitigation actions. In  
7 this study, we use the Community Atmosphere Model version 5 (CAM5) with a newly  
8 developed source tagging technique, nudged towards the MERRA meteorological reanalysis, to  
9 characterize the fate of BC particles emitted from various geographical regions and sectors.  
10 Evaluated against observations over the HTP and surrounding regions, the model simulation  
11 shows a good agreement in the seasonal variation of the near-surface airborne BC concentrations,  
12 providing confidence to use this modeling framework for characterizing BC source-receptor  
13 relationships. Our analysis shows that the relative contributions from different geographical  
14 regions and source sectors depend on season and location in the HTP. The largest contribution to  
15 annual mean BC burden and surface deposition in the entire HTP region is from biofuel and  
16 biomass (BB) emissions in South Asia, followed by fossil fuel (FF) emissions from South Asia,  
17 then FF from East Asia. The same roles hold for all the seasonal means except for the summer  
18 when East Asia FF becomes more important. For finer receptor regions of interest, South Asia  
19 BB and FF have the largest impact on BC in Himalayas and Central Tibetan Plateau, while East  
20 Asia FF and BB contribute the most to Northeast Plateau in all seasons and Southeast Plateau in  
21 the summer. Central Asia and Middle East FF emissions have relatively more important  
22 contributions to BC reaching Northwest Plateau, especially in the summer. Although local  
23 emissions only contribute about 10% of BC in the HTP, this contribution is extremely sensitive

24 to local emission changes. Lastly, we show that the annual mean radiative forcing ( $0.42 \text{ W m}^{-2}$ )  
25 due to BC in snow outweighs the BC dimming effect ( $-0.3 \text{ W m}^{-2}$ ) at the surface over the HTP.  
26 We also find strong seasonal and spatial variation with a peak value of  $5 \text{ W m}^{-2}$  in the spring  
27 over Northwest Plateau. Such a large forcing of BC in snow is sufficient to cause earlier snow  
28 melting and potentially contribute to the acceleration of glacier retreat.

29

## 30 **1 Introduction**

31 Black carbon (BC) is a distinct type of carbonaceous particulate matter mainly emitted from the  
32 incomplete combustion of fossil fuels, biofuels and biomass burning. It is the dominant insoluble  
33 light-absorbing particulate species, both in the atmosphere and after deposition on snow and ice.  
34 In addition to its impact on air quality, BC plays a unique and important role in the climate  
35 system through its effect on radiation, clouds and snow albedo, and associated feedbacks that  
36 modify atmospheric circulation patterns and/or accelerate the snowmelt and glacier retreat in the  
37 Arctic and across the mid-latitudes of the northern hemisphere (Bond et al., 2013).

38 Modeling studies (e.g., Hansen et al., 2005; Qian et al., 2011) indicate that the climate  
39 efficacy of BC in snow is much greater than efficacy of carbon dioxide or other anthropogenic  
40 forcers owing to a sequence of positive feedback mechanisms (Warren and Wiscombe, 1980,  
41 1985; Conway et al., 1996; Hansen and Nazarenko, 2004; Jacobson, 2004; Flanner et al., 2007;  
42 Ye et al., 2012; Hadley and Kirchstetter, 2012; Doherty et al., 2014). Flanner et al. (2009)  
43 demonstrated that the global annual BC snow-albedo effect (darkening) outweighs the aerosol  
44 (BC and organic matter) dimming effect (i.e., reduced the downwelling irradiance reaching the  
45 surface) by a factor of about 6. The snow/ice-covered Himalayas and Tibetan Plateau (HTP)  
46 region is more prone to these BC effects than other regions because of the surrounding two major

47 BC source regions, East Asia and South Asia, at present and likely in the future (e.g., Bond et al.,  
48 2007; Ohara et al., 2007; Xu et al., 2009; Lamarque et al., 2010; Menon et al., 2010).

49 The HTP, often referred to as the Third Pole, has received much less scientific attention  
50 than the Polar Regions (Qiu, 2008), although it is the highest and largest plateau that stores one  
51 of the largest ice masses of the Earth system. The HTP also has a large area of seasonal and  
52 permanent snow cover and represents the most sensitive and visible indicator of climate change  
53 with its unique location for complex interactions among the atmosphere, hydrosphere and  
54 cryosphere (e.g., Pu et al., 2007; Xu et al., 2009; Yao et al., 2012). The glaciers and the  
55 associated snowmelt over the HTP have a great potential to modify the regional hydrology and to  
56 trigger natural hazards that impact a large portion of the population in and around the region (e.g.,  
57 Barnett et al., 2005; Singh and Bengtsson, 2004; Xu et al., 2008; Kaser et al., 2010; Immerzeel et  
58 al., 2010; Yao et al., 2012; Bolch et al., 2012). The HTP also exerts profound influences on  
59 atmospheric circulation patterns and climate through mechanical and thermal effects due to its  
60 large area, highly elevated topography and geographical location in the Earth system (Yeh et al.,  
61 1957; Manabe and Terpstra, 1974; Ye and Gao, 1979; Yanai et al., 1992; Ye and Wu, 1998; Wu  
62 et al., 2012). The HTP acts as a giant wall across the Eurasian continent that blocks cold  
63 outbreaks from high latitudes in winter and confines the winter monsoon to eastern and southern  
64 Asia, while in summer the HTP serves as a huge heat source through the strong surface sensible  
65 heating and latent heating over central and eastern Plateau (Wu et al., 2012).

66 Under the background of global warming, the climate of the HTP is changing rapidly. For  
67 example, the surface sensible heat flux has weakened in recent decades, mainly due to global  
68 warming (Duan and Wu, 2008). Observational evidence indicated that the surface air  
69 temperatures on the HTP have increased about 1.8°C over the past 50 years (Wang et al., 2008),



70 while the large area at elevations above 4000 m has warmed at 0.3°C per decade in the past three  
71 decades (Xu et al., 2009). A number of recent studies reported that glaciers on the HTP have  
72 undergone widespread losses at an increasing rate in past decades (e.g., Qin et al., 2006; Li et al.,  
73 2008; Kang et al., 2010; Bolch et al., 2012) and have undergone accelerated retreat in recent  
74 years (Yao et al., 2007). The rapid warming and the accelerated glacier retreat have been  
75 primarily attributed to increasing greenhouse gases (e.g., Duan et al., 2006; Ren et al., 2006), but  
76 other factors may be partly responsible for the accelerated warming over the HTP, such as  
77 atmospheric heating by absorbing aerosols, land use changes, and reduction of snow albedo  
78 induced by light-absorbing impurities in snow (Kang et al., 2000; Prasad and Singh 2007;  
79 Ramanathan et al., 2007; Flanner et al., 2007, 2009; Yasunari et al., 2010; Xu et al., 2009; Qian  
80 et al., 2011, 2015). Lau et al. (2006, 2010) proposed and demonstrated the Elevated Heat Pump  
81 mechanism, whereby heating induced by airborne BC and dust absorption can strengthen local  
82 circulations and lead to a northward shift of the monsoon rain belt, widespread enhanced  
83 warming over the HTP, and accelerated snowmelt and glacier retreat. Previous observational and  
84 modeling studies have indicated that BC deposition on snow and ice, which has a rapidly  
85 increasing trend in recent years, has been a significant contributor to the early snowmelt and  
86 rapid glacier retreat over the HTP (e.g., Flanner et al., 2007, 2009; Ming et al., 2008; Xu et al.,  
87 2009; Kaspari et al., 2011; Menon, et al., 2010; Qian et al., 2011, 2015; Wang et al., 2015).  
88 Flanner et al. (2007) found that the largest regional annual mean forcing due to BC in snow is  
89 located in the HTP. Xu et al. (2009) and Lau et al. (2010) suggested that the BC in snow/ice may  
90 be partly responsible for the observed acceleration of glacier retreat in the HTP.

91 Understanding the role of BC in accelerating snow-cover reduction and glacier retreat is  
92 becoming increasingly important. Over 60% of BC in the present-day atmosphere originates

93 from anthropogenic activities (e.g., Bond et al., 2007; Lamarque et al., 2010). Reduction of  
94 emissions from BC-rich sources represents a potential mitigation strategy to slow down ~~present-~~  
95 ~~day~~ climate change because BC has a positive radiative forcing but a short atmospheric lifetime  
96 (Bond et al., 2013). Since BC over the HTP may originate from a variety of geographical regions  
97 and emission sectors, it is essential to quantify the source-receptor relationships of BC in order to  
98 understand the contributions of open fire and anthropogenic emission sectors to BC over the  
99 HTP. This exercise is also essential to provide guidance for potential mitigation actions.

100 Some studies have used the conventional back-trajectory approach to identify possible  
101 source regions for both airborne BC and that deposited on snow and ice, by tracking air mass  
102 reaching sampling sites over the HTP (e.g., Ming et al., 2008, 2009; Cao et al., 2009; Bonasoni  
103 et al., 2010; Zhao et al., 2013; Zhang et al., 2013). Lu et al. (2012) developed a novel back-  
104 trajectory approach to analyze the origin of BC transported to the HTP during 1996-2010. They  
105 derived the overall transport characteristics of BC to the HTP and showed the spatial distribution  
106 of sources for BC reaching the HTP region based on a large set of seven-day back trajectories  
107 arriving at the given height (i.e., 500 m) and receptor locations, BC emissions and transport  
108 efficiencies. The statistical analysis of trajectories has good accuracy on short time scales for  
109 source regions with close proximity to the receptor, but this approach has limitations in  
110 determining contributions from distant sources to BC in the mid- and upper-troposphere that  
111 could contribute significantly to the total column burden but less to BC deposition and boundary-  
112 layer concentrations. Using the adjoint of the GEOS-Chem global chemical transport model,  
113 Kopacz et al. (2011) attempted to identify the originating locations of BC arriving at five glacier  
114 sites (i.e., five model grid-cells as the receptors) in the HTP for year 2001. This method can  
115 provide a global distribution of emissions that directly contribute to BC concentrations at

Hailong Wang 5/10/2015 10:35 PM

Deleted: the

117 receptor locations. Note that the adjoint model results are not source attributions but rather the  
118 source-receptor sensitivities, which can be interpreted as the effectiveness of incremental  
119 changes to existing emissions in affecting BC at receptor locations. While the adjoint approach  
120 has the advantage of not predefining source regions, it does require performing separate  
121 simulations for each of the defined receptor regions.

122 In this study, we use an aerosol-climate model with a newly developed explicit source  
123 tagging approach (Wang et al., 2014) to produce a detailed characterization of the fate of BC  
124 emitted from various geographical regions and sectors (e.g., fossil fuel, biofuel and biomass  
125 burning emissions) and transport pathways to the HTP. In contrast to the back-trajectory and the  
126 adjoint approaches, the direct tagging method has the flexibility to do source attribution of BC  
127 mass mixing ratio at any model layer and the surface dry and/or wet deposition within a single  
128 simulation for any receptor regions. Section 2 describes the aerosol-climate model and the  
129 tagging method used in this study. Section 3 presents an evaluation of modeled BC surface  
130 concentrations and seasonal snow cover over the HTP region. The transport pathways and source  
131 attribution results are presented in Sect. 4. The radiative effects of BC in the atmosphere and of  
132 both BC and mineral dust in snow are compared in Sect. 5, followed by the summary and  
133 conclusions in Sect. 6.

134

## 135 **2 Model Configuration and Experimental Design**

### 136 **2.1 The CAM5 model and the source-tagging method**

137 We use the Community Atmosphere Model Version 5 (CAM5; Neale et al., 2012), which is the  
138 atmospheric component of the Community Earth System Model version 1 (CESM1) (Hurrell et  
139 al., 2013). It includes relatively comprehensive representations of aerosols and clouds, and

140 mechanisms for their interactions with each other and with climate (Gettelman et al., 2010; Liu  
141 et al., 2012). CAM5 employs a modal aerosol module (MAM) to represent aerosols in multiple  
142 log-normally distributed modes, with internal mixing assumed for aerosol species within each  
143 individual mode, including a 3-mode standard representation (MAM3) and a more complex 7-  
144 mode representation (MAM7). The major difference between MAM3 and MAM7 related to  
145 carbonaceous aerosols lies in the treatment of aging. In MAM3, BC and primary organic matter  
146 (POM) particles are emitted into the accumulation mode that also contains highly hygroscopic  
147 species such as sulfate and sea-salt, while in MAM7 BC and POM are emitted into a primary  
148 carbon mode, which contains no other species. BC is hydrophobic upon emission, and thus the  
149 hygroscopicity of the primary-carbon-mode particles depends on the assumed hygroscopicity for  
150 POM. As more hygroscopic species (e.g., H<sub>2</sub>SO<sub>4</sub> and NH<sub>3</sub>) condense onto the primary-carbon-  
151 mode particles, the particles are become more hygroscopic and are gradually transferred into the  
152 MAM7 accumulation mode. The rate of transfer is controlled by uncertain aging parameters, and  
153 the availability of gas precursors (Liu et al. 2012). In the accumulation mode of both MAM3 and  
154 MAM7, BC is internally mixed with other more hygroscopic species and is thus subject to wet  
155 scavenging and removal processes. During the transport from sources to remote regions, aerosols  
156 are removed too efficiently in the default CAM5 (Liu et al., 2012). Recently, H. Wang et al.  
157 (2013) revised some key processes associated with aerosol wet removal and convective transport,  
158 which significantly improved the vertical distribution of aerosols and their transport to remote  
159 regions such as the Arctic.

160 To better characterize the sensitivity of BC spatial distributions to emission uncertainties,  
161 Wang et al. (2014) implemented a direct source tagging method in CAM5, whereby BC emitted  
162 from a number of independent source regions and/or sectors can be tagged and explicitly tracked

163 within a single model simulation. This approach provides the quantitative characterization of  
164 source-receptor relationships for BC in any receptor region without perturbing emissions from  
165 individual BC source regions or sectors. In this study, we apply the BC tagging technique to the  
166 accumulation-mode BC in the MAM3 treatment. BC particles emitted from sixteen geographical  
167 BC source regions and two emissions sectors (i.e., biomass burning & biofuel emissions and  
168 fossil fuel emissions) in each of the regions are tagged and explicitly tracked. Instead of using  
169 the global emissions from all sectors for the original one BC mass mixing ratio variable, the  
170 thirty two regional/sectoral emissions provide sources to the respective tagged BC mass mixing  
171 ratio variables that are all added to the accumulation mode, including both interstitial and cloud-  
172 borne states. All physical and dynamic tendencies (e.g., transport, dry and wet removal) are  
173 calculated explicitly for the tagged BC mass mixing ratio variables in the same way as the  
174 original single BC mass mixing ratio. Also, when aerosol optical properties are calculated, all of  
175 the tagged BC mass mixing ratios contribute to the volume-mean refractive index of the  
176 accumulation mode that is used in the radiation calculation.

177 In addition to the free-running mode, CAM5 can also be configured in an offline mode,  
178 in which temperature, wind, surface fluxes (heat, moisture, and momentum), and pressure are  
179 constrained to agree closely with observations, while clouds and aerosol are allowed to evolve  
180 freely (Rasch et al., 1997; Lamarque et al., 2012; Ma et al., 2013). In this study, we run the  
181 CAM5 model in the offline mode with the direct BC source tagging capability, including the  
182 improved representation of convective transport and wet removal of aerosols. We use the NASA  
183 Modern Era Retrospective-Analysis for Research and Applications (MERRA) reanalysis dataset  
184 (Rienecker et al., 2011), using a horizontal resolution of  $1.9^\circ \times 2.5^\circ$  and 56 vertical levels. The  
185 goal is to characterize the fate of BC emitted from various geographical regions and sectors, their

186 transport pathways to the HTP, and their radiative forcing with seasonal variations. The  
187 simulation is performed for year 2001 with prescribed sea surface temperatures.

## 188 **2.2 BC source regions and sectors**

189 BC emission datasets have large uncertainties (e.g., Bond et al., 2013), and there are different  
190 inventories available for climate modeling. We use the present-day (i.e., year 2000) monthly  
191 mean emission inventories for BC provided by Lamarque et al. (2010). They were built for the  
192 climate model simulations in the Coupled Model Intercomparison Project Phase 5 (CMIP5)  
193 (Taylor et al., 2012) performed for the fifth assessment report (AR5) of the Intergovernmental  
194 Panel on Climate Change (IPCC). The AR5 BC emissions being used in our CAM5 simulation  
195 include monthly varying elevated open fire emissions (injection altitude up to 6 km), and yearly  
196 constant surface emissions from shipping and from six sectors over land: agricultural waste  
197 burning, domestic, energy, industry, transportation, and waste treatment. These surface BC  
198 emissions sectors do not distinguished between biofuel and fossil fuel combustion. To prepare  
199 for the BC source sector tagging, we divide the total surface emissions into two broader sectors,  
200 biofuel and fossil fuel, by using the ratio of biofuel to biofuel plus fossil fuel at each model grid  
201 provided by Dentener et al. (2006). We then combine the biomass burning (open fire) emissions  
202 and surface biofuel emissions, hereafter, referred to as BB (biofuel and biomass) sector. The  
203 shipping emissions are combined with the fossil fuel emissions over land to form the FF (fossil  
204 fuel) sector. Note that emissions in the BB sector have seasonal variations (associated with the  
205 open fire emissions) but the FF sector emissions used in this study have no seasonal variation at  
206 all.

207 The sixteen geographical BC source regions (Fig. 1a) are defined using the definition of  
208 source/receptor regions by Work Plan (WP 2.1) of the Task Force on Hemispheric Transport of

209 Air Pollution (<http://iek8wikis.iek.fz-juelich.de/HTAPWiki/WP2.1>). They are ARC (Arctic),  
210 NAM (North America), CAM (Central America), SAM (South America), EUR (Europe), NAF  
211 (North Africa), SAF (South Africa), MDE (Middle East), CAS (Central Asia), SAS (South Asia),  
212 EAS (East Asia), SEA (South East Asia), PAN (Pacific, Australia and New Zealand), RBU  
213 (Russia, Belarus and Ukraine), HTP (Himalayas and Tibetan Plateau) and ROW (Rest of World).

214 Figure 1b and Table S1 in the Supplement summarize the fractional contributions of BC  
215 emissions from the different source regions and sectors. The global annual mean BC emission  
216 rate is  $7.78 \text{ Tg yr}^{-1}$ , with 56.2% (sum of the red bars) from BB emissions (33.6% from fires and  
217 22.6% from biofuel) and 43.8% (sum of the blue bars) from FF emissions. The two largest  
218 contributors are BB emissions from SAF (about 20%) and FF emissions from EAS (about 15%),  
219 followed by BB emissions from SEA (7.7%), EAS (6.4%), SAS (6.2%) and SAM (5.7%), and  
220 EUR FF (6.4%) emissions. The geographical distributions of BC annual mean emission fluxes  
221 from BB and FF sectors for year 2000 are shown in Fig. S1 (in Supplement). The global annual  
222 and seasonal mean lifetime of BC emitted from the tagged source regions and sectors are  
223 summarized in Table S2. On the globe average, BB BC has a longer lifetime than FF BC in all  
224 seasons, especially in boreal winter (6.9 vs. 3.1 day), due in part to higher open-fire emissions (in  
225 the BB sector) during local dry seasons. Another reason is that open-fire emissions have initial  
226 injection heights of up to 6 km, resulting in less removal below 6 km. The availability of co-  
227 emitted hygroscopic species that are internally mixed with BC in the accumulation mode of the  
228 MAM3 aerosol treatment also impacts the scavenging and wet removal rate of BC. This also in  
229 part explains the variability of BC lifetime among the different source regions and sectors.  
230 Regarding the seasonal cycle, BC emitted from the major source regions (e.g., SAF, EAS, SEA,

231 SAS) has substantially lower lifetime in summer (JJA) than in the other seasons, likely due to  
 232 relatively strong removal by the summer monsoon precipitation.

233 We use two metrics for quantifying source-receptor relationships and the sensitivity of  
 234 BC in a receptor region to various sources following Wang et al. (2014), but we extend them to  
 235 treat BB and FF sectors separately.

236 1) The fractional contribution of BB and FF emissions from source region  $i$  to a BC property in  
 237 receptor region  $j$  (the entire HTP or a subset of it),  $C_i^{BB}$  or  $C_i^{FF}$ , is defined as

$$238 \quad C_i^{BB} = \frac{A_i^{BB}}{A_j}, C_i^{FF} = \frac{A_i^{FF}}{A_j} \quad (1)$$

239 Where  $A_i^{BB}$  and  $A_i^{FF}$  are a BC property (e.g., mass mixing ratio, column burden, or deposition  
 240 flux) in/over receptor region  $j$  resulting from BB and FF emissions, respectively, in source region  
 241  $i$ , and  $A_j = \sum_{i=1}^N (A_i^{BB} + A_i^{FF})$  represents the total BC property in the receptor region from all  
 242 source regions ( $N = 16$  in this study) and sectors (BB and FF). Note that for BC properties such  
 243 as column burden, surface mixing ratio, and deposition flux, the tagging method in CAM5  
 244 explicitly calculates how much is due to emissions from each source region and sector.

245 2) The efficiency of BB and FF emissions from source region  $i$  in changing BC in a receptor  
 246 region  $j$  is defined as

$$247 \quad S_i^{BB} = \frac{C_i^{BB}}{E_i^{BB}/E_{tot}}, S_i^{FF} = \frac{C_i^{FF}}{E_i^{FF}/E_{tot}} \quad (2)$$

248 Where  $C_i^{BB}$  and  $C_i^{FF}$  are the fractional contribution defined in Eq. (1), and  $E_i^{BB}$  and  $E_i^{FF}$  are the  
 249 total BB and FF emission rates, respectively, in source region  $i$ , and  $E_{tot} = \sum_{i=1}^N (E_i^{BB} + E_i^{FF})$  in  
 250 Eq. (2) represents the global total emission rate. The efficiency metric  $S_i^{BB}$  or  $S_i^{FF}$  characterizes  
 251 the sensitivity of aerosol properties in a receptor region to per unit (BB or FF) emissions in  
 252 source region  $i$ . As noted in Wang et al. (2014), the efficiency is proportional to the metric of

Hailong Wang 5/9/2015 2:09 PM

Deleted: the

Hailong Wang 5/10/2015 9:54 PM

Deleted:  $\sum_{i=1}^N (A_i^{BB} + A_i^{FF})$

Hailong Wang 5/10/2015 9:55 PM

Deleted:  $\sum_{i=1}^N (A_i^{BB} + A_i^{FF})$

Hailong Wang 5/9/2015 2:11 PM

Deleted: the

Hailong Wang 5/9/2015 2:17 PM

Deleted: .

Hailong Wang 5/9/2015 2:17 PM

Deleted: The summation

Hailong Wang 5/9/2015 2:15 PM

Deleted: E

Hailong Wang 5/10/2015 10:00 PM

Deleted:  $\left[ \frac{E_i^{BB}}{\sum_{i=1}^N (E_i^{BB} + E_i^{FF})} \right]$

Hailong Wang 5/10/2015 10:01 PM

Deleted:  $\left[ \frac{E_i^{FF}}{\sum_{i=1}^N (E_i^{BB} + E_i^{FF})} \right]$

Hailong Wang 5/9/2015 2:19 PM

Deleted: . The summation

Hailong Wang 5/9/2015 2:20 PM

Deleted: also

Hailong Wang 5/9/2015 2:21 PM

Deleted: the

Hailong Wang 5/9/2015 2:21 PM

Deleted: the



266 [relative contribution per unit source region emission used by Shindell et al. \(2008\). Physically,](#)  
267 [the efficiency metric can be viewed as the efficiency of transport from a source region to the](#)  
268 [receptor region.](#) This metric is [perhaps](#) of more interest to policy makers for the purpose of  
269 mitigation action, which is not the focus of this study but is worth mentioning.

270

### 271 **3 Model evaluation against available observations**

272 The CAM5 model has been evaluated in detail from different perspectives with available  
273 observations such as aerosol mass concentration, aerosol number concentration and size  
274 distribution, aerosol optical properties, cloud properties, aerosol deposition and BC in snow over  
275 various regions in previous studies (Liu et al., 2012; H. Wang et al., 2013; Ma et al., 2013; Jiao  
276 et al., 2014; Lee et al., 2013; Qian et al., 2014). Because of the complex topography and  
277 meteorology of the HTP and the relatively coarse resolution of global model, further model  
278 evaluation focusing on the HTP region is critical. Here we use near-surface atmospheric BC  
279 concentrations measured at a few HTP sites and the snow cover fraction retrieved from satellite  
280 to evaluate the CAM5 performance in the HTP.

#### 281 **3.1 Atmospheric BC surface concentration**

282 There are seven remote sites that have surface measurements of seasonal BC aerosol  
283 concentrations available. The locations and elevations of the sites and the sampling time periods  
284 and observation methods are described in Table 1. Figure 2 shows the comparison of seasonal  
285 mean BC concentrations between observations and CAM5 results. Note that model results  
286 represent mean concentrations in the grid box that the sampling sites reside in and at the grid-  
287 mean elevation, which could deviate significantly from the sampling point near complex terrain.  
288 All sites have non-negligible amounts of BC in the near-surface air. The error bars indicate the

289 intra-seasonal and inter-annual variations if multi-year data were used for given season and site.  
290 However, the uncertainties of observed BC surface concentrations mainly originate from the  
291 large discrepancies between different measurement methods, the mixing of BC with other  
292 components (e.g., organic carbon and mineral dust) in the aerosol samples, and the sampling  
293 time and location (Bond et al., 2013; Petzold et al., 2013). BC surface concentrations over the  
294 various sites show strong seasonal variations, which are reasonably captured by the model. The  
295 modeled magnitude of BC concentrations has a good agreement with observations at some sites  
296 (e.g., Fig. 2b, d, g), but the model clearly overestimates BC at the Muztagh Ata site (Fig. 2a) and  
297 underestimates at the Lulang site (Fig. 2e). The large underestimation (about 1000 m; see Table  
298 1) of the Muztagh Ata site elevation in the model, determined by the model grid resolution, could  
299 largely explain the overestimation of BC since BC concentrations have sharp decreases with  
300 height in this region. At the sites over southern HTP (i.e., Hanle, Manora Peak, NCO-P, Lulang  
301 and NCOS), the BC surface concentrations in the summer (JJA) are lower, mainly due to wet  
302 scavenging by more frequent precipitation and partly due to the minimal emissions from  
303 domestic heating and wildfires over Himalaya foothills and Indo-Gangetic Plains (IGP) during  
304 the Indian summer monsoon season (Marinoni et al., 2010, 2013). Among all these sites, the  
305 largest BC surface concentrations occur at the Manora Peak site that is closer to the major  
306 sources in South Asia, especially in the winter (DJF) when the model underestimates the  
307 concentrations by about 50%. The high concentrations in winter at Manora Peak is mainly due to  
308 the dry winter monsoon conditions and increased transport of emissions from regional biomass  
309 burning, agricultural waste and wood fuel burning from the IGP (e.g., Ram et al., 2010; Moorthy  
310 et al., 2013). The BC surface concentrations peak in the springtime (MAM) at Hanle, NCO-P,  
311 Lulang and NCOS sites. This might be related to an increase in BB and/or FF emissions in the

312 Indian Subcontinent, along with the higher regional boundary-layer top over the IGP during the  
313 springtime that may favor the transport of particles from the surface up to higher altitudes (e.g.,  
314 Marinoni et al., 2010, 2013). Moreover, a long-range transport of pollution emitted from distant  
315 regions like the Middle East, North Africa or Europe (Marinoni et al., 2010) could further  
316 contribute to BC variability over the South Himalayas, which will also be examined in this study.  
317 Part of the discrepancies between observations and model results can be attributed to the inherent  
318 difficulty in simulating the cloud/precipitation fields over the complex topography and  
319 subsequent wet removal of aerosols during the transport, but emission uncertainties (e.g., Bond  
320 et al., 2013) might play a primary role.

### 321 **3.2 Snow cover fraction**

322 It is important to evaluate the performance of model in simulating seasonal snow over this region  
323 in order to assess the importance of BC-in-snow effect. Figure 3 shows the CAM5 simulated  
324 seasonal and annual mean snow cover fraction (SCF) during year 2001, in comparison to  
325 observed mean SCF, derived from the Moderate Resolution Imaging Spectrometer (MODIS)  
326 (Hall et al., 2006) monthly mean of daily products at 0.05 degree resolution. For a better  
327 comparison, the MODIS monthly mean SCFs are mapped to the CAM5 grid. The summer (JJA)  
328 season only includes July and August for both CAM5 and MODIS due to missing MODIS data  
329 in June 2001. To illustrate whether year 2001 can represent the average condition in terms of  
330 SCF, the MODIS SCF climatology (2000-2013) is also plotted. The overall SCF in HTP has very  
331 small difference between climatology and year 2001 in all seasons except for JJA, when SCF is  
332 notably higher over northwest Plateau for the climatology that included June SCF in the average.  
333 On average, SCF is about 5% (absolute amount) higher in June than in July and August. Over the  
334 52 HTP grid cells, the CAM5 SCF is highly correlated spatially with that of MODIS (for both

335 2001 and 2000-2013) with the statistical confidence level greater than 99%, except for summer  
336 (JJA) when the linear correlation is significant only at 80% level.

337         There are strong spatial and seasonal variations in SCF due to the complex terrain and  
338 seasonal variation in snowfall and melting. The SCF over the entire HTP reaches the maximum  
339 in the winter (DJF), while decreases to almost none (less than 5%) in July and August. Snow  
340 covers the western and southeastern Plateau during the transition seasons (MAM and SON). The  
341 CAM5 simulation shows a good agreement with MODIS in the annual mean (ANN) SCF and the  
342 strong seasonality. The most persistent snow cover at the southern and western edges of the HTP  
343 and the relatively less persistent in the HTP interior are captured by the CAM5 model. The  
344 performance of the CAM5 has been improved, in comparison to its earlier version (CAM3) that  
345 remarkably overestimated the SCF especially over the HTP interior (Qian et al., 2011), although  
346 the CAM5 still significantly overestimates the SCF in the western Plateau in DJF and MAM and  
347 underestimates it in JJA. The CAM3 model used by Qian et al. (2011) overestimates SCF by up  
348 to a factor of 2 during the cold season (November to April). The CAM3 spring (MAM) mean  
349 SCF is greater than 35%, while the CAM5 spring mean (21%) in the present study is in good  
350 agreement with the MODIS spring SCF ( $18\pm 5\%$ ).

351         Although we believe that the CAM5 SCF biases are qualitatively robust, it is worth  
352 noting that the MODIS products have uncertainties as well. Pu et al. (2007) evaluated the  
353 MODIS SCF products over the HTP against ground-based snow observations and showed that  
354 total error in MODIS SCF products over the HTP is about 10%. However, their analysis based  
355 on MODIS eight-day snow-cover composite gave a significantly higher SCF (more than 10%)  
356 than the one we show here using daily products, especially, in winter and early spring.  
357 Interestingly, based on a different source of observation, Qin et al. (2006) found that snow covers

358 about 59% of the Tibetan Plateau in winter, which is comparable to the mean SCF (50%) in our  
359 CAM5 simulation. Nonetheless, we keep this discrepancy in mind when interpreting the  
360 wintertime BC-in-snow radiative forcing that suffers the most from such potential SCF bias.

361

## 362 **4 Modeled transport pathways and source attribution of BC in the HTP**

### 363 **4.1 Transport pathways**

364 The direct source tagging method can clearly characterize the three-dimensional transport  
365 pathways of BC emitted from various source regions and sectors to the HTP receptor region.  
366 General circulation patterns over the HTP and surroundings are typically affected by mid-latitude  
367 westerlies in the winter and Asian monsoon in the summer, including the South Asian summer  
368 monsoon and East Asian summer monsoon (Xu et al., 2009; Yao et al., 2012; Wu et al., 2012;  
369 also see Fig. S2).

370 Figure 4 illustrates circulation patterns over HTP and BC transport pathways from six  
371 major source regions to the HTP in the winter (DJF) and summer (JJA). (See similar plots in  
372 Figs. S3–S5 for other tagged source regions.) In the winter, the strong surface cooling over the  
373 HTP leads to subsidence/divergence and the formation of an enhanced local circulation cell,  
374 while in the summer air converges toward the HTP from the surroundings, particularly from the  
375 South Asia, due to the ascending of strongly heated air over the HTP (e.g., Wu et al., 2012), as  
376 also indicated by the arrows in the vertical cross-sections in Fig. 4. In the winter, the subtropical  
377 westerlies extend to about 10°N in mid-/upper troposphere and 20°N near surface, and the  
378 tropical easterlies are weak (see the white contours of latitude-height cross-section panels in Fig.  
379 4). The circulation patterns near the HTP change dramatically during the summer monsoon

380 season. The reversal of surface wind regime in the tropics (e.g., Arabian Sea, Bay of Bengal, and  
381 South China Sea) is characteristic of the Asian summer monsoon climate (see Fig. S2e, g). The  
382 subtropical westerlies recede to north of 30°N and the center of the westerly jet shifts to about  
383 40°N in JJA (from about 30°N in DJF). The strong easterlies characterize the upper troposphere  
384 of tropical region (south of HTP), while the southwesterly flow prevails in the lower troposphere  
385 (white contours of latitude-height cross-section panels in Fig. 4). The prevailing winds during the  
386 transition seasons (MAM and SON) between DJF and JJA are still westerlies (Fig. S2b, d).

387         The circulation patterns determine the transport of BC around the HTP region. However,  
388 the variations of spatial distributions of BC emitted from the different source regions and in  
389 different seasons could be due to the differences in source location and strength, wet removal  
390 rate and lifting. Note that although we combined BC emitted from BB and FF sections to  
391 characterize transport pathways in Fig. 4, only BC emissions from BB sector have seasonal  
392 variations in the emission inventory we use.

393         The HTP region is surrounded by two major BC source regions, SAS and EAS (Fig. 1a),  
394 which potentially have great impact on BC in the HTP (e.g., Menon et al., 2010; Bond et al.,  
395 2007; Ohara et al., 2007; Xu et al., 2009; Kopacz et al., 2011; Lu et al., 2012). BC emissions  
396 from SAS are dominated by the BB sector, and by FF sector from EAS (Fig. 1b). As shown in  
397 Fig. 4, in the winter, a significant amount of BC from SAS can be transported to the eastern  
398 Plateau by the strong westerlies under the dry winter monsoon conditions. During the South  
399 Asian summer monsoon BC from SAS is effectively removed by the local abundant  
400 precipitation, as indicated by the low lifetime in summer (Table S2), but can still affect large area  
401 in the southwest of the HTP. However, BC from EAS can be uplifted higher and transported  
402 more to the Northeast Plateau in the summer monsoon season than in the winter. Along the

403 | wintertime westerlies, BC from upwind source regions (e.g., EUR, NAF, SAF, MDE, and CAS;  
404 | [see Fig. S3](#)) can easily move to the HTP, while the HTP local emissions are transported far away  
405 | (Fig. 4). BC originating from the distant sources such as SAF and MDE reaches up high (to  
406 | 300hPa) in the HTP. In the summer, continental deep convection can loft BC into higher  
407 | altitudes where it can be transported to the HTP along the relatively weaker westerlies from  
408 | upwind source regions (e.g., EUR, RBU, MDE, and CAS; [see Figs. 4 and S3](#)). However, BC  
409 | from distant low-latitude source regions such as SAF barely reaches the HTP region due to weak  
410 | emissions but strong removal along the transport pathways to the HTP during the summer  
411 | monsoon season.

#### 412 | **4.2 Seasonal variation of BC in the HTP**

413 | BC concentrations in the HTP have strong dependence on season and location. Figure 5 shows  
414 | the annual mean and seasonal variations of BC column burden and deposition rate over the HTP  
415 | and five sub-regions. The seasonal variation of the ratio of wet to total BC deposition is  
416 | superimposed. The Central Plateau is the cleanest region during all seasons, compared to other  
417 | sub-regions in the HTP (Fig. 5e). Both BC column burden and deposition rate from the BB  
418 | sector peak in MAM over the HTP, mostly in the Himalayas and Southeast Plateau region. The  
419 | FF BC burden in the HTP peaks in the summer mainly due to the seasonal maximum over  
420 | Northwest and Northeast Plateaus. However, BC wet removal rate over the Northwest Plateau is  
421 | at minimum in the summer, as opposed to the summer maximum in other sub-regions and the  
422 | entire HTP region. For Himalayas, Southeast and Central Plateau, the seasonal variation (i.e.,  
423 | maximum in MAM followed by a sharp decrease to JJA) of BB and FF column burden (Fig. 5c,  
424 | d and e) is similar to the variation of observed surface concentrations at sites located in these  
425 | sub-regions (Fig. 2b, d, e and f). In the Himalayas and Southeast Plateau, the ratio of regional

426 mean BC column burden to deposition rate (Fig. 5c and d), indicator of removal time scale or  
427 lifetime, is the smallest (less than 1 day) during the Asian summer monsoon (JJA) due to the  
428 efficient wet scavenging of BC by abundant precipitation. In Northwest and Northeast Plateau,  
429 the BC column burden increases from DJF to JJA and reaches the maximum in JJA, and then  
430 decreases in SON (Fig. 5b and f), partly due to the peak contribution of EAS and CAS emissions  
431 in JJA. This trend is also similar to that in the observed surface concentrations (Fig. 2a and g).  
432 The deposition rate follows the same seasonal variation of column burden over the Northeast  
433 Plateau, while the deposition has a minimum in JJA over the Northwest Plateau when the column  
434 burden is at maximum likely due to the less efficient wet removal in this region (Fig. 5b and f).

435 The annual mean BC column burden over the HTP has almost the same contributions  
436 from BB and FF emission origins, with BB dominating in DJF and MAM and FF in JJA. In the  
437 Himalayas, BC is predominantly from BB sector for all seasons (Fig. 5c). In the Southeast and  
438 Central Plateaus, the dominant source sector is BB in DJF and MAM, but FF dominates in JJA.  
439 The dominant source sector over the Northwest and Northeast Plateaus is always FF, especially  
440 in the summer. We need to analyze the source-receptor relationships in order to quantify the  
441 roles of BB and FF emissions from the various source regions in determining BC over the HTP  
442 and the sub-regions.

#### 443 **4.3 BC source-receptor relationships**

444 Previous studies (e.g., Xu et al., 2009; Kopacz et al., 2011) have shown that BC and its source-  
445 receptor relationships vary significantly with season and location in the HTP. We intend to  
446 quantify source contributions to BC at different locations of the HTP and in different seasons.  
447 Our analysis also shows that the relative contributions to BC from different source regions and



448 sectors depend on season and location in the HTP. As shown in Fig. 6, the largest contribution to  
449 the annual mean BC burden and surface deposition for the entire HTP region is from BB  
450 emissions from SAS, followed by FF emissions from SAS and then the FF from EAS. The same  
451 roles hold for all the seasonal means except for the summer (JJA) when the EAS FF becomes  
452 more important for BC column burden in the HTP and, to a lesser extent, for deposition.

453 The SAS emissions account for 50% of the annual mean burden over the HTP, including  
454 33% from BB and 17% from FF. The other 50% is mostly from the EAS (5% BB and 14% FF),  
455 HTP (6% BB and 6% FF), CAS FF (4%), MDE FF (4%) and SAF BB (3%). The source  
456 attribution for annual mean BC deposition for the entire HTP is similar, but SAS contributes  
457 even more to BC deposition than to the column burden. Although RBU has a lower contribution  
458 to the annual mean BC in the HTP than the six regions shown in Fig. 6, its contribution to the  
459 JJA mean, especially at some locations, is quite substantial (included in the black bar) and even  
460 more important than some of the six regions in Fig. 6, as discussed in detail below.

461 BC annual mean burden over the HTP has nearly equal contributions from BB and FF  
462 emissions. However, contribution by BB emissions, mainly from SAS, is larger than from FF  
463 sector in DJF and MAM. In the summer (JJA), the largest contribution (about 29%) to HTP BC  
464 is from EAS FF emissions. This is partly due to the change of circulation patterns (Fig. 4) and  
465 effective wet removal of SAS BB emissions. Note that EAS FF emissions are much larger than  
466 FF emissions from any other of the source regions, and are more than twice the EAS BB  
467 emissions.

468 For BC in the five finer receptor regions of interest (as defined in Fig. 5g), SAS BB and  
469 FF have the largest contribution to BC in Himalayas and Central Plateau, while EAS FF and BB

470 contribute the most to Northeast Plateau in all seasons and Southeast Plateau in the summer.  
471 Central Asia and Middle East FF emissions have relatively more important contribution to BC  
472 reaching Northwest Plateau, especially in the summer.

473 For the Northwest Plateau (Fig. 6b), the prevailing winds in this sub-region are westerly  
474 throughout the year (Fig. S2; Cao et al., 2009; Xu et al., 2009), so the important source regions  
475 ought to locate at the west of HTP (e.g., MDE, EUR, and parts of SAS and RBU in Fig. 1a). SAS  
476 emissions are still the dominant source for the annual BC burden in this sub-region (17% from  
477 BB and 14% from FF), followed by HTP local emissions (9% from BB and 13% from FF), CAS  
478 (2% from BB and 14% from FF), MDE FF (8%) and EAS FF (7%). BC emissions from SAS are  
479 the dominant source in DJF, MAM and SON. CAS becomes the dominant source region (5%  
480 from BB and 26% from FF) in JJA, even though CAS is not a significant emission source region  
481 on a global basis (Fig. 1b). BC emitted from MDE is predominantly in the FF sector throughout  
482 the year. Emissions from the rest of the tagged sources (in addition to the top six) become more  
483 significant in this sub-region (black color in Fig. 6b), mostly from EUR and RBU through long-  
484 range transport (Fig. S3). The source attribution for BC deposition in this sub-region is similar to  
485 that of the column burden, but BC emitted from SAS and MDE appears to be more efficient in  
486 deposition except for the JJA season when BC from EAS contributes more to deposition than to  
487 column burden.

488 The Himalayas sub-region located along the southern edge of the HTP is in close  
489 proximity to the SAS. Thus emissions from SAS are absolutely the dominant source for BC in  
490 Himalayas throughout the year. This sub-region receives more BC from BB sector than FF  
491 because BC emissions in SAS are mainly in the BB sector, especially in MAM season (Fig. 1b  
492 and Fig. S6). For the annual mean burden, BC from SAS contributes 81% (54% from BB and

493 27% from FF), followed by HTP local emissions (6% from BB and 3% from FF). It is worth  
494 noting that SAF BB emissions contribute about 10% to burden in DJF through a long-range  
495 transport. BC deposition in this sub-region also predominantly originates from SAS, which is  
496 consistent with previous studies by Ming et al. (2008) and Kopacz et al. (2011).

497 For the Southeast Plateau (Fig. 6d), the BC source contribution profile is similar to that of  
498 Himalayas during DJF and MAM season, in which SAS is still the dominant source, especially  
499 in MAM (74% contribution to column burden, including 53% from BB and 21% from FF),  
500 although the contribution from EAS is larger here than for the Himalayas. As also pointed by  
501 Ramanathan et al. (2007), BC over the SAS can be transported to the Southeast Plateau by the  
502 southern branch of the westerlies during the winter and spring. However, the BC source  
503 contribution profile changes dramatically during the summer when emissions in EAS become the  
504 dominant source to this sub-region (68% to column burden, including 23% from BB and 45%  
505 from FF). Kopacz et al. (2011) also found that the BC from south-eastern China is the dominant  
506 contributor to the Southeast Plateau in July. For the annual mean burden in this sub-region, SAS  
507 is still the dominant contributor (40% from BB and 17% from FF), followed by EAS (8% from  
508 BB and 15% from FF), HTP (6% from BB and 6% from FF). BC originating from EAS  
509 contributes more to deposition than to burden in this sub-region.

510 For the Central Plateau (Fig. 6e), source attribution profiles for annual and seasonal BC  
511 are very similar to those of the entire HTP region with SAS being the dominant source region  
512 throughout the year except that EAS has comparable contributions in JJA. Ming et al. (2010)  
513 pointed out that pollutants from the Indo-Gangetic Basin could be transported to the Central  
514 Plateau by both the summer monsoon and the westerlies. Xia et al. (2011) also found that the  
515 substantial regional atmospheric brown haze from the nearby regions of SAS is the main source

516 for the background aerosols in the Central Plateau based on sunphotometer and satellite  
517 observations.

518 Compared to the other sub-regions, the Northeast Plateau receives the largest contribution  
519 of BC from EAS throughout the year (50% to annual mean burden, including 12% from BB and  
520 38% from FF; see Fig. 6f), especially in JJA (17% from BB and 49% from FF). The EAS FF  
521 sector contribution and the magnitude of burden (Fig. 5f) over the Northeast Plateau have strong  
522 seasonal variations, mostly due to variations in meteorology because the FF emissions in our  
523 simulation do not vary seasonally. Kopacz et al. (2011) indicate that the primary contribution to  
524 BC over the Northeast Plateau is from western China during January and April (transported by  
525 mid-tropospheric westerlies), and from central-eastern China during July and October  
526 (transported by boundary layer flow). Other main contributions to BC burden over the Northeast  
527 Plateau include 13% from SAS and 10% from HTP local emissions. Similar to the Northwest  
528 Plateau, some other upwind source regions (e.g., CAS, MDE, RBU and EUR; [see Figs. 4 and S3](#))  
529 have a significant contribution to the Northeast sub-region as well.

#### 530 **4.4 Seasonal variation of HTP BC sensitivity**

531 Following Wang et al. (2014), we defined the “efficiency” metric in Sect. 2.2 to quantify the  
532 sensitivity of BC response to absolute change (e.g., per unit perturbation) of emissions in  
533 different source regions. This metric has the value of 1 if the entire globe is treated as a single  
534 source region, so we may assume the global mean efficiency of 1 as a reference to measure the  
535 sensitivity to perturbation from different source regions/sectors.

536 Figure 7 shows efficiencies of tagged sources in affecting the BC seasonal and annual  
537 mean column burden and deposition in the HTP and five sub-regions (as defined in Fig. 5g). BC

538 in the same receptor regions is generally most sensitive to change in local emissions, regardless  
539 of seasons, emission sectors and locations of receptor regions. Among all the source regions,  
540 although the HTP local (FF+BB) emissions only contribute about 10%, BC in the HTP is  
541 extremely sensitive to changes in the emissions within HTP (not shown in the figure), mainly  
542 because the emission rate is very low. In addition to the local emissions, BC in the HTP is also  
543 sensitive to emissions in neighboring source regions (e.g., SAS and CAS) and emissions from  
544 distant sources such as MDE. Not only does the SAS have large contribution to BC burden and  
545 deposition over the HTP, as well as most of the sub-regions except for the Northeast Plateau  
546 (receptor V), but also the efficiencies for SAS emissions are high for almost all of the sub-  
547 regions especially the Himalayas (receptor II). BC in the Northeast Plateau (receptor V) is quite  
548 sensitive to EAS emissions in all seasons, while BC in the Southeast Plateau is sensitive to EAS  
549 emissions in JJA and SON. Although BC emissions from MDE and CAS are weak (Fig. 1b) and  
550 their contributions to the HTP are relatively low, their efficiencies are high. BC over Northwest  
551 Plateau (receptor I) and Central Plateau (receptor IV) is extremely sensitive to emissions from  
552 CAS in JJA. These source-receptor relationships of sensitivity will provide useful information  
553 for policymakers to improve the effective mitigation road map in order to potentially slow down  
554 the glacier retreat in the HTP region.

555

## 556 **5 Radiative forcing**

557 The BC-in-snow effect can be quantified using the online calculation of radiative forcing in the  
558 SNICAR (Snow, Ice, and Aerosol Radiative) model (Flanner et al., 2007) coupled to CAM5, and  
559 then compared to airborne BC radiative forcing. Figure 8 shows seasonal and annual mean BC

560 all-sky shortwave direct radiative forcing (DRF) at the surface (dimming) and the top of the  
561 atmosphere (TOA), and the BC-in-snow radiative forcing (darkening) averaged over the entire  
562 HTP and the five sub-regions (as defined in Fig. 5g). Note that the BC-in-snow forcing is  
563 averaged over all model grids in the area (i.e., zero enters the calculation for any grid when snow  
564 is not present). The radiative forcing of BC (and dust) in snow is small in JJA and SON due to a  
565 lack of snow cover (Fig. 3). The forcing maximum occurs during the spring melt (MAM) when  
566 the insolation is rather intense and BC accumulates at the surface of the snowpack as the snow  
567 melts (Conway et al., 1996; Flanner et al., 2007, 2009), and when the snow-albedo feedback is  
568 strongest (Hall and Qu, 2006). This strong seasonal variation also explains why the coefficient of  
569 variation (i.e., the ratio of the SD to the mean) is greater than 1 for the annual mean BC-in-snow  
570 forcing over the entire HTP and all sub-regions. The seasonal variations of airborne BC DRF at  
571 the TOA and surface are consistent with that of the BC column burden (Fig. 5). For the entire  
572 HTP (Fig. 8a1), the annual mean surface radiative forcing due to BC in snow ( $0.42 \text{ W m}^{-2}$ )  
573 exceeds the BC dimming effect at the surface ( $-0.3 \text{ W m}^{-2}$ ). The annual mean BC-in-snow  
574 forcing is even higher over the Northwest Plateau (Fig. 8b1) and Himalayas (Fig. 8c1), and far  
575 exceeds the other forcings in the same sub-regions, although the BC-in-snow effect may be  
576 overestimated due to the potential positive bias in snow cover fraction in our simulation (Fig. 3).  
577 The annual mean BC surface dimming exceeds the BC-in-snow effect in the Southeast (Fig. 8d1),  
578 Central (Fig. 8e1) and Northeast Plateau (Fig. 8f1). The minima of all BC-related forcings  
579 appear in the Central Plateau where the BC burden and deposition are the lowest among all the  
580 sub-regions (Fig. 5), and the SCF is very small (Fig. 3).

581 We have also calculated an approximate source attribution for the BC-in-snow radiative  
582 forcing over the HTP and its sub-regions, using the tagged-source BC deposition, which is

583 simply assumed to be linearly proportional to BC-in-snow radiative forcing. The SCF is taken  
584 into account in the calculation (i.e., the deposition at each model grid is multiplied by SCF when  
585 calculating the area-average deposition). Overall, despite small quantitative differences, the  
586 source contributions to BC-in-snow forcing are similar to those for BC deposition (Fig. 6). The  
587 SAS BB emissions contribute the most to annual mean forcing over the HTP and sub-regions  
588 except for the Northeast Plateau that is mostly contributed by EAS FF emissions. During the  
589 winter and spring seasons over Northwest Plateau and Himalayas, when and where the forcing is  
590 the largest, SAS (especially the BB sector) is the major contributor.

591 Dust is a major contributor to the total aerosol burden over the HTP (e.g., Zhang et al.,  
592 2001). Although we don't focus on other snow impurities such as mineral dust, it is worth noting  
593 that dust-in-snow radiative forcing has been considered in our model simulation and it could be  
594 an important forcing agent. We also plotted dust-in-snow forcing over the HTP and sub-regions  
595 in Fig. 8 (along with the BC-induced forcings). The annual mean dust-in-snow forcing ( $0.33 \text{ W}$   
596  $\text{m}^{-2}$ ) is comparable to all of the other forcings over the HTP, especially in the springtime when  
597 dust outbreaks and can be transported to the HTP from the surrounding sources such as  
598 Taklimakan and Gobi deserts (Liu et al., 2008). The annual mean dust-in-snow forcing is as large  
599 as  $0.99$  and  $0.59 \text{ W m}^{-2}$  in the Northwest and Northeast Plateau, respectively (Fig. 8b1 and f1),  
600 which is in close proximity to the Taklimakan Desert (Huang et al., 2007; Chen et al., 2013), but  
601 negligibly small in the Southeast Plateau and Central Plateau. In the winter, the dominant dust in  
602 snow effect over Northeast Plateau is consistent with the recent observations. Huang et al. (2011),  
603 X. Wang et al. (2013) and Zhang et al. (2013) found that insoluble light-absorbing particles in  
604 snow are dominated by local soil and desert dust in the Qilian Mountain (Northeast Plateau).

605 Both snow cover fraction (SCF) and mass concentration of snow impurities affect the  
606 calculation of radiative forcing in snow. We have evaluated the model estimation of SCF in  
607 different seasons (Fig. 3). We have also compared BC concentration and deposition flux from  
608 our model results to a recent modeling study by Ménégóz et al. (2014) and to observations in the  
609 HTP (Ginot et al., 2014) (Table S3). Bond et al. (2013) pointed out that observations of BC in  
610 snow pits or ice cores mostly involve snow/ice samples obtained in the summer and early fall,  
611 when almost all grid boxes the sample sites located in are snow free in the HTP. They also  
612 indicated that the CAM3 global climate model (Flanner et al., 2009) may be overestimating snow  
613 BC concentrations in the HTP, especially in the spring. Our comparison shows that despite a  
614 smaller bias than in Ménégóz et al. (2014) the CAM5 model still largely overestimates BC  
615 concentrations in snow but underestimates dust concentrations in snow over the HTP. Ménégóz  
616 et al. (2014) provided a few possible reasons for the differences between model simulations and  
617 observations. Factors such as measurement uncertainties (due to sample treatment and analysis  
618 methodology), temporal (inter-annual and seasonal) and spatial variations of BC deposition, and  
619 vertical variations of BC in snowpack, can strongly affect the accuracy and representativeness of  
620 BC-in-snow measurements for the purpose of evaluating global models. Ming et al. (2013) and  
621 Qian et al. (2015) pointed out that BC concentrations in snow and ice samples over HTP tend to  
622 decrease with increasing glacier elevations, while global models with coarse grid resolution  
623 cannot accurately represent elevation of sampling sites. Often times the difference is significant.  
624 Nonetheless, it is likely that positive biases exist in the modeled concentration and radiative  
625 forcing of BC and dust in snow.

## 626 **6 Summary and conclusions**



627 In this study, we employed the CAM5 model with a newly developed source tagging technique,  
628 nudged towards the MERRA meteorological reanalysis, to characterize the fate of BC particles  
629 emitted from various geographical regions and sectors to the HTP region. In addition, we  
630 compare the radiative forcing induced by BC in the atmosphere and in snow over the HTP, as  
631 well as forcing induced by dust in snow. Although there are biases in the simulated BC, partly  
632 due to the inherent difficulty for coarse-resolution global models to accurately represent transport  
633 and wet deposition in this topographically complex region, the CAM5 model simulation shows a  
634 reasonable agreement in the seasonal variation of the near-surface airborne BC concentrations  
635 with observations over the HTP and surrounding regions. This provides us the confidence to use  
636 this modeling framework to characterize BC source-receptor relationships in the HTP. Using  
637 very different approaches, Kopacz et al. (2011), Lu et al. (2012) and the present study all show  
638 that South Asia and East Asia are the main source regions for BC transported to the HTP, while  
639 the magnitude of contributions from each of the source regions varies with season and receptor  
640 location. Although all of the three studies can provide quantitative source attributions, a  
641 quantitative inter-comparison of the findings is quite difficult, given the differences in the  
642 definition of geographical source and receptor regions, emission inventories, time periods for  
643 model simulation, and analysis methods. Nevertheless, in addition to quantifying the  
644 contributions of source regions, our direct source tagging approach allows us to further break  
645 down regional contributions by sectors (i.e., fossil fuel vs. biomass & biofuel) and to characterize  
646 the transport pathways of individual regional/sectoral emissions.

647 The explicit source tagging technique enables the characterization of three-dimensional  
648 transport pathways of BC to the HTP from different geographical regions and source sectors,  
649 which also depends on seasons and the location of the receptor in the HTP. With the IPCC AR5

650 present-day emission inventories, the annual mean BC column burden and surface deposition in  
651 the entire HTP region is contributed the most by biomass and biofuel (BB) emissions from South  
652 Asia (SAS) (33% and 40%, respectively), followed by fossil fuel (FF) emissions from SAS (17%  
653 and 20%, respectively), and then the FF from East Asia (EAS) (14% and 14%, respectively). The  
654 same roles hold for all the seasonal means except for the summer when the EAS FF becomes  
655 more important. Although BC emissions from the entire EAS source region are much stronger  
656 than those from SAS, the concentrated FF BC emissions in central-eastern China are only  
657 transported towards the HTP during the East Asian summer monsoon. Thus seasonal prevailing  
658 winds are important in determining the seasonal variations in BC transport and source-receptor  
659 relationships.

660 Both the annual and seasonal mean BC properties and their source-receptor relationships  
661 vary significantly with location in the HTP. For the multiple finer receptor regions of interest,  
662 SAS BB and FF have the largest impact on BC in Himalayas and Central Plateau, while EAS FF  
663 and BB contribute the most to Northeast Plateau in all seasons and Southeast Plateau in the  
664 summer. The Central Asia (CAS) and Middle East (MDE) FF emissions make important  
665 contributions to BC over the Northwest Plateau, especially from CAS in JJA.

666 The HTP BC is most sensitive by far to per unit changes in the local emissions, although  
667 they only contribute about 10% to the BC burden in the HTP. The SAS region makes large  
668 contributions to BC burden and deposition over the HTP and the BC sensitivities to SAS  
669 emissions are also high for almost all of the sub-regions of HTP, especially the Himalayas. BC  
670 over the Northeast Plateau is quite sensitive to EAS emissions in all seasons, and Southeast  
671 Plateau BC is also sensitive to EAS emissions in JJA. Although BC emissions from MDE and  
672 CAS are weak and their contribution to the HTP overall is low, their efficiencies are quite high.

673 BC over Northwest Plateau and Central Plateau is extremely sensitive to emissions from CAS in  
674 JJA. These source-receptor relationships and sensitivities can be useful to policymakers for  
675 improving the effective mitigation road map in order to potentially slow down the glacier retreat  
676 in the HTP region.

677 The impact of BC on snow and glacier melting can be characterized by the magnitude of  
678 radiative forcing. Our calculations show that the annual mean BC-in-snow radiative forcing ( $0.42$   
679  $W m^{-2}$ ) outweighs BC dimming effect ( $-0.3 W m^{-2}$ ) at the surface over the HTP. In the five sub-  
680 regions, the annual mean BC-in-snow forcing ranges from  $0.04 W m^{-2}$  in the Central Plateau to  
681  $1.75 W m^{-2}$  in the Northwest Plateau. We also showed that the annual mean dust-in-snow  
682 induced radiative forcing over the HTP can be quite significant ( $0.33 W m^{-2}$  for entire the HTP,  
683 and  $0.99 W m^{-2}$  for the Northwest Plateau). More importantly, both BC- and dust-in-snow  
684 forcing peaks in the spring melting season when the area-average forcing reaches  $1.03$  and  $0.87$   
685  $W m^{-2}$ , respectively, over the entire HTP, and their combined forcing is more than  $8 W m^{-2}$  over  
686 the Northwest Plateau. Such a large forcing is sufficient to cause earlier snow melting and  
687 contribute to the acceleration of glacier retreat, although the model is likely to overestimate BC-  
688 in-snow forcing due to the possible positive bias of snow cover fraction in the winter and early  
689 spring. According to our estimates of the source attribution, the biomass burning and biofuel  
690 emissions in South Asia contribute the most to annual mean forcing over the HTP and its sub-  
691 regions except for the Northeast Plateau where the largest contribution is from East Asia fossil  
692 fuel emissions. During the winter and spring seasons over Northwest Plateau and Himalayas,  
693 when and where the forcing is the largest, South Asia (especially the biomass burning and  
694 biofuel sector) is the major contributor.

695

696 *Acknowledgments.* This research is based on work supported by the U.S. Department of Energy (DOE),  
697 Office of Science, Biological and Environmental Research as part of the Earth System Modeling  
698 Program. The Pacific Northwest National Laboratory (PNNL) is operated for DOE by Battelle Memorial  
699 Institute under contract DE-AC05-76RLO1830. The CESM project is supported by the National Science  
700 Foundation and the DOE Office of Science. R. Zhang acknowledges support from the China Scholarship  
701 Fund. J. Huang and Q. Fu acknowledge support from the National Basic Research Program of China  
702 (2012CB955303), NSFC grant 41275070 and China 111 project (No. B13045). Computational resources  
703 were provided by the National Energy Research Scientific Computing Center (NERSC), a national  
704 scientific user facility located at Lawrence Berkeley National Laboratory in Berkeley, California. NERSC  
705 is the flagship scientific computing facility for the Office of Science in DOE.

706

## 707 **References**

- 708 Babu, S. S., Chaubey, J. P., Moorthy, K. K., Gogoi, M. M., Kompalli, S. K., Sreekanth, V., Bagare, S. P., Bhatt, B.  
709 C., Gaur, V. K., Prabhu, T. P., and Singh, N. S.: High altitude (~4520 m amsl) measurements of black  
710 carbon aerosols over western trans-Himalayas: Seasonal heterogeneity and source apportionment, *J.*  
711 *Geophys. Res.*, 116, D24201, doi:10.1029/2011JD016722, 2011.
- 712 Barnett, T. P., Adam, J. C., and Lettenmaier, D. P.: Potential impacts of a warming climate on water availability in  
713 snow-dominated regions, *Nature*, 438, 303–309, doi:10.1038/Nature04141, 2005.
- 714 Bolch, T., Kulkarni, A., Käab, A., Huggel, C., Paul, F., Cogley, J., Frey, H., Kargel, J., Fujita, K., Scheel, M.,  
715 Bajracharya, S., and Stoffel, M.: The state and fate of Himalayan Glaciers, *Science*, 336, 310–314,  
716 doi:0.1126/science.1215828, 2012.
- 717 Bond, T. C., Bhardwaj, E., Dong, R., Jogani, R., Jung, S., Roden, C., Streets, D. G., and Trautmann, N. M.:  
718 Historical emissions of black and organic carbon aerosol from energy-related combustion, 1850–2000,  
719 *Global Biogeochem. Cy.*, 21, GB2018, doi:10.1029/2006GB002840, 2007.
- 720 Bond, T. C., Doherty, S. J., Fahey, D. W., Forster, P. M., Berntsen, T., DeAngelo, B. J., Flanner, M. G., Ghan, S.,  
721 Kärcher, B., Koch, D., Kinne, S., Kondo, Y., Quinn, P. K., Sarofim, M. C., Schultz, M. G., Schulz, M.,  
722 Venkataraman, C., Zhang, H., Zhang, S., Bellouin, N., Guttikunda, S. K., Hopke, P. K., Jacobson, M. Z.,  
723 Kaiser, J. W., Klimont, Z., Lohmann, U., Schwarz, J. P., Shindell, D., Storelvmo, T., Warren, S. G., and  
724 Zender, C. S.: Bounding the role of black carbon in the climate system: A scientific assessment, *J. Geophys.*  
725 *Res.-Atmos.*, 118, 5380–5552, doi:10.1002/jgrd.50171, 2013.
- 726 Bonasoni, P., Laj, P., Marinoni, A., Sprenger, M., Angelini, F., Arduini, J., Bonaf'e, U., Calzolari, F., Colombo, T.,  
727 Decesari, S., DiBiagio, C., di Sarra, A. G., Evangelisti, F., Duchi, R., Facchini, MC., Fuzzi, S., Gobbi, G. P.,  
728 Maione, M., Panday, A., Roccatò, F., Sellegri, K., Venzac, H., Verza, GP., Villani, P., Vuillermoz, E., and  
729 Cristofanelli, P.: Atmospheric Brown Clouds in the Himalayas: first two years of continuous observations  
730 at the Nepal Climate Observatory-Pyramid (5079 m), *Atmos. Chem. Phys.*, 10, 7515–7531,  
731 doi:10.5194/acp-10-7515-2010, 2010.

- 732 Cao, J. J., Xu, B. Q., He, J. Q., Liu, X. Q., Han, Y. M., Wang, G. H., and Zhu, C. S.: Concentrations, seasonal  
733 variations, and transport of carbonaceous aerosol at a remote Mountainous region in western China, *Atmos.*  
734 *Environ.*, 43, 4444–4452, doi:10.1016/j.atmosenv.2009.06.023, 2009.
- 735 Chen, S., J. Huang, C. Zhao, Y. Qian, L. R. Leung, and B. Yang: Modeling the Transport and Radiative Forcing of  
736 Taklimakan Dust over the Tibetan Plateau in Summer, *J. Geophys. Res.*, 118, 797–812,  
737 doi:10.1002/jgrd.50122, 2013.
- 738 Conway, H., Gades, A., and Raymond, C. F.: Albedo of dirty snow during conditions of melt, *Water Resour. Res.*,  
739 32, 1713–1718, doi:10.1029/96WR00712, 1996.
- 740 Dentener, F., Kinne, S., Bond, T., Boucher, O., Cofala, J., Generoso, S., Ginoux, P., Gong, S., Hoelzemann, J. J., Ito,  
741 A., Marelli, L., Penner, J. E., Putaud, J.-P., Textor, C., Schulz, M., van der Werf, G. R., and Wilson, J.:  
742 Emissions of primary aerosol and precursor gases in the years 2000 and 1750 prescribed data-sets for  
743 AeroCom, *Atmos. Chem. Phys.*, 6, 4321–4344, doi:10.5194/acp-6-4321-2006, 2006.
- 744 Doherty, S. J., Dang, C., Hegg, D. A., Zhang, R., and Warren, S. G.: Black carbon and other light-absorbing  
745 particles in snow of central North America, *J. Geophys. Res. Atmos.*, 119, 12,807–12,831,  
746 doi:10.1002/2014JD022350, 2014.
- 747 Duan, A., Wu G., Zhang Q., and Liu Y.: New proofs of the recent climate warming over the Tibetan Plateau as a  
748 result of the increasing greenhouse gases emissions, *Chin. Sci. Bull.*, 51, 1396–1400, doi:10.1007/s11434-  
749 006-1396-6, 2006.
- 750 Duan, A. M. and Wu G. X.: Weakening trend in the atmospheric heat source over the Tibetan Plateau during recent  
751 decades. Part I: Observations, *J. Clim.*, 21, 3149–3164, doi:10.1175/2007JCLI1912.1, 2008.
- 752 Flanner, M. G., Zender, C. S., Randerson, J. T., and Rasch, P. J.: Present day climate forcing and response from  
753 black carbon in snow, *J. Geophys. Res.*, 112, D11202, doi:10.1029/2006JD008003, 2007.
- 754 Flanner, M. G., Zender, C. S., Hess, P. G., Mahowald, N. M., Painter, T. H., Ramanathan, V., and Rasch, P. J.:  
755 Springtime warming and reduced snow cover from carbonaceous particles, *Atmos. Chem. Phys.*, 9, 2481–  
756 2497, doi:10.5194/acp-9-2481-2009, 2009.
- 757 Gettelman, A., Liu, X., Ghan, S. J., Morrison, H., Park, S., Conley, A. J., Klein, S. A., Boyle, J., Mitchell, D. L., and  
758 Li, J. L. F.: Global simulations of ice nucleation and ice supersaturation with an improved cloud scheme in  
759 the Community Atmosphere Model, *J. Geophys. Res.*, 115, D18216, doi:10.1029/2009jd013797, 2010.
- 760 Ginot, P., Dumont, M., Lim, S., Patris, N., Taupin, J.-D., Wagnon, P., Gilbert, A., Arnaud, Y., Marinoni, A.,  
761 Bonasoni, P., and Laj, P.: A 10 year record of black carbon and dust from a Mera Peak ice core (Nepal):  
762 variability and potential impact on melting of Himalayan glaciers, *The Cryosphere*, 8, 1479-1496,  
763 doi:10.5194/tc-8-1479-2014, 2014.
- 764 Hadley, O. L. and Kirchstetter, T.W.: Black-carbon reduction of snow albedo, *Nat. Clim. Change*, 2, 437–440, 2012.
- 765 Hall, D. K., Riggs G. A., and Salomonson V. V.: updated monthly. MODIS/TERRA Snow Cover Monthly L3  
766 Global 0.05Deg CMG V005, [2001], Boulder, CO, National Snow and Ice Data Center. Digital Media,  
767 distributed in netCDF format by the Integrated Climate Data Center (ICDC, <http://icdc.zmaw.de> University  
768 of Hamburg, Hamburg, Germany), 2006.
- 769 Hall, A. and Qu, X.: Using the current seasonal cycle to constrain snow albedo feedback in future climate change,  
770 *Geophys. Res. Lett.*, 33, L03502, doi:10.1029/2005GL025127, 2006.

- 771 Hansen, J. and Nazarenko, L.: Soot climate forcing via snow and ice albedos, *P. Natl. Acad. Sci. USA*, 101, 423–  
772 428, doi:10.1073/pnas.2237157100, 2004.
- 773 Hansen, J., Sato, M., Ruedy, R., Nazarenko, L., Lacis, A., Schmidt, G. A., Russell, G., Aleinov, I., Bauer, M., Bauer,  
774 S., Bell, N., Cairns, B., Canuto, V., Chandler, M., Cheng, Y., Del Genio, A., Faluvegi, G., Fleming, E.,  
775 Friend, A., Hall, T., Jackman, C., Kelley, M., Kiang, N., Koch, D., Lean, J., Lerner, J., Lo, K., Menon, S.,  
776 Miller, R., Minnis, P., Novakov, T., Oinas, V., Perlwitz, Ja., Perlwitz, Ju., Rind, D., Romanou, A., Shindell,  
777 D., Stone, P., Sun, S., Tausnev, N., Thresher, D., Wielicki, B., Wong, T., Yao, M., and Zhang, S.: Efficacy  
778 of climate forcings, *J. Geophys. Res.*, 110, D18104, doi:10.1029/2005JD005776, 2005.
- 779 Huang, J., Minnis, P., Yi, Y., Tang, Q., Wang, X., Hu, Y., Liu, Z., Ayers, K., Trepte, C., and Winker, D.: Summer  
780 dust aerosols detected from CALIPSO over the Tibetan Plateau, *Geophys. Res. Lett.*, 34, L18805,  
781 doi:10.1029/2007GL029938, 2007.
- 782 Huang, J., Fu, Q., Zhang, W., Wang, X., Zhang, R., Ye, H., and Warren, S. G.: Dust and black carbon in seasonal  
783 snow across Northern China, *Bull. Am. Meteorol. Soc.*, 92, 175–181, doi:10.1175/2010BAMS3064.1, 2011.
- 784 Hurrell, J. W., Holland, M. M., Ghan, S., Lamarque, J.-F., Lawrence, D., Lipscomb, W. H., Mahowald, N., Marsh,  
785 D., Rasch, P., Bader, D., Collins, W. D., Gent, P. R., Hack, J. J., Kiehl, J., Kushner, P., Large, W. G.,  
786 Marshall, S., Vavrus, S., and Vertenstein, M.: The Community Earth System Model: A Framework for  
787 Collaborative Research, *Bull. Am. Meteorol. Soc.*, 94, 1339-1360, doi:10.1175/BAMS-D-12-00121, 2013.
- 788 Immerzeel, W., VanBeek L. P. H., and Bierkens, M. F. P.: Climate Change Will Affect the Asian Water Towers,  
789 *Science*, 328, 1382–1385, doi:10.1126/science.1183188, 2010.
- 790 Jacobson, M. Z.: Climate response of fossil fuel and biofuel soot, accounting for soot’s feedback to snow and sea ice  
791 albedo and emissivity, *J. Geophys. Res.*, 109, D21201, doi:10.1029/2004JD004945, 2004.
- 792 Jiao, C., Flanner, M. G., Balkanski, Y., Bauer, S. E., Bellouin, N., Bernsten, T. K., Bian, H., Carslaw, K. S.,  
793 Chin, M., De Luca, N., Diehl, T., Ghan, S. J., Iversen, T., Kirkevåg, A., Koch, D., Liu, X., Mann, G. W.,  
794 Penner, J. E., Pitari, G., Schulz, M., Seland, Ø., Skeie, R. B., Steenrod, S. D., Stier, P., Takemura, T.,  
795 Tsigaridis, K., van Noije, T., Yun, Y., and Zhang, K.: An AeroCom assessment of black carbon in Arctic  
796 snow and sea ice, *Atmos. Chem. Phys.*, 14, 2399-2417, doi:10.5194/acp-14-2399-2014, 2014.
- 797 Kang, S., Wake C., Qin, D., Mayewski P. A., and Yao T.: Monsoon and dust signals recorded in Dasuopu glacier,  
798 Tibetan Plateau, *J. Glaciol.*, 46(153), 222–226, 2000.
- 799 Kang, S., Wei, X., You, Q., Flugel, W., Pepin, N., and Yao, T.: Review of climate and cryospheric change in the  
800 Tibetan Plateau, *Environ. Res. Lett.*, 5, 015101, doi:10.1088/1748-9326/5/1/015101, 2010.
- 801 Kaser, G., Grosshauser, M., and Marzeion, B.: Contribution of glaciers to water availability in different climate  
802 regimes, *P. Natl. Acad. Sci. USA*, 107, 20223–20227, doi:10.1073/pnas.1008162107, 2010
- 803 Kaspari, S. D., Schwikowski, M., Gysel, M., Flanner, M. G., Kang, S., Hou, S., and Mayewski, P. A.: Resent  
804 increase in black carbon concentrations from a Mt. Everest ice core spanning 1860–2000 AD, *Geophys.*  
805 *Res. Lett.*, 38, L04703, doi:10.1029/2010GL046096, 2011.
- 806 Kopacz, M., Mauzerall, D. L., Wang, J., Leibensperger, E. M., Henze, D. K., and Singh, K.: Origin and radiative  
807 forcing of black carbon transported to the Himalayas and Tibetan Plateau, *Atmos. Chem. Phys.*, 11, 2837-  
808 2852, doi:10.5194/acp-11-2837-2011, 2011.

- 809 Lamarque, J.-F., Bond, T. C., Eyring, V., Granier, C., Heil, A., Klimont, Z., Lee, D., Liousse, C., Mieville, A.,  
810 Owen, B., Schultz, M. G., Shindell, D., Smith, S. J., Stehfest, E., Van Aardenne, J., Cooper, O. R.,  
811 Kainuma, M., Mahowald, N., McConnell, J. R., Naik, V., Riahi, K., and van Vuuren, D. P.: Historical  
812 (1850–2000) gridded anthropogenic and biomass burning emissions of reactive gases and aerosols:  
813 methodology and application, *Atmos. Chem. Phys.*, 10, 7017–7039, doi:10.5194/acp-10-7017-2010, 2010.
- 814 Lamarque, J. F., Emmons, L. K., Hess, P. G., Kinnison, D. E., Tilmes, S., Vitt, F., Heald, C. L., Holland, E. A.,  
815 Lauritzen, P. H., Neu, J., Orlando, J. J., Rasch, P. J., and Tyndall, G. K.: CAM-chem: description and  
816 evaluation of interactive atmospheric chemistry in the Community Earth System Model, *Geosci. Model  
817 Dev.*, 5, 369–411, doi:10.5194/gmd-5-369-2012, 2012.
- 818 Lau, K. M., Kim, M. K., and Kim, K. M.: Asian monsoon anomalies induced by aerosol direct forcing: the role of  
819 the Tibetan Plateau, *Clim. Dyn.*, 26, 855–664, 2006.
- 820 Lau, K.-M., Kim, M. K., Kim, K.-M., and Lee, W. S.: Enhanced surface warming and accelerated snow melt in the  
821 Himalayas and Tibetan Plateau induced by absorbing aerosols, *Environ. Res. Lett.*, 5, 025204  
822 doi:10.1088/1748-9326/5/2/025204, 2010.
- 823 Lee, Y. H., Lamarque, J.-F., Flanner, M. G., Jiao, C., Shindell, D. T., Berntsen, T., Bisiaux, M. M., Cao, J.,  
824 Collins, W. J., Curran, M., Edwards, R., Faluvegi, G., Ghan, S., Horowitz, L. W., McConnell, J. R.,  
825 Ming, J., Myhre, G., Nagashima, T., Naik, V., Rumbold, S. T., Skeie, R. B., Sudo, K., Takemura, T.,  
826 Thevenon, F., Xu, B., and Yoon, J.-H.: Evaluation of preindustrial to present-day black carbon and its  
827 albedo forcing from Atmospheric Chemistry and Climate Model Intercomparison Project (ACCMIP),  
828 *Atmos. Chem. Phys.*, 13, 2607-2634, doi:10.5194/acp-13-2607-2013, 2013.
- 829 Li, X., Cheng, G., Jin, H., Kang, E., Che, T., Jin, R., Wu, L., Nan, Z., Wang, J., and Shen, Y.: Cryospheric change in  
830 China, *Global Planet. Change*, 62(3–4), 210–218, 2008.
- 831 Liu, X., Easter, R. C., Ghan, S. J., Zaveri, R., Rasch, P., Shi, X., Lamarque, J.-F., Gettelman, A., Morrison, H., Vitt,  
832 F., Conley, A., Park, S., Neale, R., Hannay, C., Ekman, A. M. L., Hess, P., Mahowald, N., Collins, W.,  
833 Iacono, M. J., Bretherton, C. S., Flanner, M. G., and Mitchell, D.: Toward a minimal representation of  
834 aerosols in climate models: description and evaluation in the Community Atmosphere Model CAM5,  
835 *Geosci. Model Dev.*, 5, 709–739, doi:10.5194/gmd-5-709-2012, 2012.
- 836 Liu, Z., Liu, D., Huang, J., Vaughan, M., Uno, I., Sugimoto, N., Kittaka, C., Trepte, C., Wang, Z., Hostetler, C., and  
837 Winker, D.: Airborne dust distributions over the Tibetan Plateau and surrounding areas derived from the  
838 first year of CALIPSO lidar observations, *Atmos. Chem. Phys.*, 8, 5045-5060, doi:10.5194/acp-8-5045-  
839 2008, 2008.
- 840 Lu, Z., Streets, D. G., Zhang, Q., and Wang, S.: A novel back-trajectory analysis of the origin of black carbon  
841 transported to the Himalayas and Tibetan Plateau during 1996–2010, *Geophys. Res. Lett.*, 39, L01809,  
842 doi:10.1029/2011GL049903, 2012.
- 843 Ma, P.-L., Rasch, P. J., Wang, H., Zhang, K., Easter, R. C., Tilmes, S., Fast, J. D., Liu, X., Yoon, J.-H., and  
844 Lamarque, J.-F.: The role of circulation features on black carbon transport into the Arctic in the  
845 Community Atmosphere Model Version 5 (CAM5), *J. Geophys. Res. - Atmos.*, 118, 4657–4669, 2013.
- 846 Manabe, S., and Terpstra T. B.: The effects of mountains on the general circulation of the atmosphere as identified  
847 by numerical experiments, *J. Atmos. Sci.*, 31, 3–42, 1974.

848 Marinoni, A., Cristofanelli, P., Laj, P., Duchi, R., Calzolari, F., Decesari, S., Sellegri, K., Vuillermoz, E., Verza, G.  
849 P., Villani, P., and Bonasoni, P.: Aerosol mass and black carbon concentrations, a two year record at NCO-  
850 P (5079 m, Southern Himalayas), *Atmos. Chem. Phys.*, 10, 8551–8562, doi:10.5194/acp-10-8551-2010,  
851 2010.

852 Marinoni, A., Cristofanelli, P., Laj, P., Duchi, R., Putero, D., Calzolari, F., Landi, T. C., Vuillermoz, E., Maione, M.,  
853 and Bonasoni, P.: High black carbon and ozone concentrations during pollution transport in the Himalayas:  
854 Five years of continuous observations at NCO-P global GAW station, *J. Environ. Sci.*, 25, 1618–1625,  
855 doi:10.1016/S1001-0742(12)60242-3, 2013.

856 Ménégoz, M., Krinner, G., Balkanski, Y., Boucher, O., Cozic, A., Lim, S., Ginot, P., Laj, P., Gallée, H., Wagnon, P.,  
857 Marinoni, A., and Jacobi, H. W.: Snow cover sensitivity to black carbon deposition in the Himalayas: from  
858 atmospheric and ice core measurements to regional climate simulations, *Atmos. Chem. Phys.*, 14, 4237-  
859 4249, doi:10.5194/acp-14-4237-2014, 2014.

860 Menon, S., Koch, D., Beig, G., Sahu, S., Fasullo, J., and Orlikowski, D.: Black carbon aerosols and the third polar  
861 ice cap, *Atmos. Chem. Phys.*, 10, 4559–4571, doi:10.5194/acp-10-4559-2010, 2010.

862 Ming, J., Cachier, H., Xiao, C., Qin, D., Kang, S., Hou, S., and Xu, J.: Black carbon record based on a shallow  
863 Himalayan ice core and its climatic implications, *Atmos. Chem. Phys.*, 8, 1343–1352, doi:10.5194/acp-8-  
864 1343-2008, 2008.

865 Ming, J., Xiao, C. D., Cachier, H., Qin, D. H., Qin, X., Li, Z. Q., and Pu, J. C.: Black carbon (BC) in the snow of  
866 glaciers in west China and its potential effects on albedos, *Atmos. Res.*, 92, 114–123,  
867 doi:10.1016/j.atmosres.2008.09.007, 2009.

868 Ming, J., Xiao C., Sun J., Kang S., and Bonasoni P.: Carbonaceous particles in the atmosphere and precipitation of  
869 the Nam Co region, central Tibet, *J. Environ. Sci.*, 22(11), 1748–1756, doi:10.1016/S1001-0742(09)60315-  
870 6, 2010.

871 Ming, J., Xiao, C., Du, Z., and Yang, X.: An overview of black carbon deposition in High Asia glaciers and its  
872 impacts on radiation balance, *Adv. Water Resour.*, 55, 80–87, 2013.

873 Moorthy, K. K., Beegum, S. N., Srivastava, N., Satheesh, S. K., Chin, M., Blond, N., Babu, S. S., and Singh, S.:  
874 Performance evaluation of chemistry transport models over India, *Atmos. Environ.*, 71, 210–225, 2013.

875 Neale, R. B., Chen, C.-C., Gettelman, A., Lauritzen, P. H., Park, S., Williamson, D. L., Conley, A. J., Garcia, R.,  
876 Kinnison, D., Lamarque, J.-F., Marsh, D., Mills, M., Smith, A. K., Tilmes, S., Vitt, F., Cameron-Smith, P.,  
877 Collins, W. D., Iacono, M. J., Easter, R. C., Ghan, S. J., Liu, X., Rasch, P. J., and Taylor, M. A.:  
878 Description of the NCAR Community Atmosphere Model (CAM 5.0), NCAR/TN-486+STR, available at:  
879 [http://www.cesm.ucar.edu/models/cesm1.0/cam/docs/description/cam5\\_desc.pdf](http://www.cesm.ucar.edu/models/cesm1.0/cam/docs/description/cam5_desc.pdf) (last access: 26 December  
880 2014), 2012.

881 Ohara, T., Akimoto, H., Kurokawa, J., Horii, N., Yamaji, K., Yan, X., and Hayasaka, T.: An Asian emission  
882 inventory of anthropogenic emission sources for the period 1980–2020, *Atmos. Chem. Phys.*, 7, 4419–4444,  
883 doi:10.5194/acp-7-4419-2007, 2007.

884 Petzold, A., Ogren, J. A., Fiebig, M., Laj, P., Li, S.-M., Baltensperger, U., Holzer-Popp, T., Kinne, S.,  
885 Pappalardo, G., Sugimoto, N., Wehrli, C., Wiedensohler, A., and Zhang, X.-Y.: Recommendations for  
886 reporting "black carbon" measurements, *Atmos. Chem. Phys.*, 13, 8365–8379, doi:10.5194/acp-13-8365-  
887 2013, 2013.



- 888 Prasad, A. K. and Singh, R. P.: Changes in Himalayan Snow and Glacier Cover Between 1972 and 2000, *Eos Trans.*  
889 *AGU*, 88, 33, doi:10.1029/2007EO330002, 2007.
- 890 Pu, Z., Xu L., and Salomonson V. V.: MODIS/Terra observed seasonal variations of snow cover over the Tibetan  
891 Plateau, *Geophys. Res. Lett.*, 34, L06706, doi:10.1029/2007GL029262, 2007.
- 892 Qian, Y., Flanner, M. G., Leung, L. R., and Wang, W.: Sensitivity studies on the impacts of Tibetan Plateau  
893 snowpack pollution on the Asian hydrological cycle and monsoon climate, *Atmos. Chem. Phys.*, 11, 1929-  
894 1948, doi:10.5194/acp-11-1929-2011, 2011.
- 895 Qian, Y., Wang H., Zhang R., Flanner M. G., and Rasch P. J.: A sensitivity study on modeling black carbon in snow  
896 and its radiative forcing over the Arctic and Northern China, *Environ. Res. Lett.*, 9, 064001,  
897 doi:10.1088/1748-9326/9/6/064001, 2014.
- 898 Qian, Y., Yasunari, T. J., Doherty, S. J., et al., Light-absorbing particles in snow and ice: measurement and  
899 modeling of climatic and hydrological impact. *Adv. Atmos. Sci.*, 32(1), 64-91 doi: 10.1007/s00376-014-  
900 0010-0, 2015.
- 901 Qin, D., Liu, S., and Li, P.: Snow cover distribution, variability, and response to climate change in western China, *J.*  
902 *Clim.*, 19(9), 1820–1833, 2006.
- 903 Qiu, J.: China: the third pole. *Nature News*, 454(7203), 393-396, 2008.
- 904 Ram, K., Sarin, M. M., and Hegde, P.: Long-term record of aerosol optical properties and chemical composition  
905 from a high-altitude site (Manora Peak) in Central Himalaya, *Atmos. Chem. Phys.*, 10, 11791–11803,  
906 doi:10.5194/acp-10-11791-2010, 2010.
- 907 Ramanathan, V., Ramana, M. V., Roberts, G., Kim, D., Corrigan, C., Chung, C., Winker, D.: Warming trends in  
908 Asia amplified by brown clouds solar absorption, *Nature*, 448, 575–578, 2007.
- 909 Rasch, P. J., Mahowald, N. M., and Eaton, B. E.: Representations of transport, convection, and the hydrological  
910 cycle in chemical transport models: Implications for the modeling of short-lived and soluble species, *J.*  
911 *Geophys. Res.*, 102, 28 127–28 138, 1997.
- 912 Ren, J., Jing, Z., Pu, J., and Qin, X.: Glaciers variations and climate change in the central Himalaya over the past  
913 few decades, *Ann. Glaciol.*, 43, 218–222, 2006.
- 914 Rienecker, M. M., Suarez, M. J., Gelaro, R., Todling, R., Bacmeister, J., Liu, E., Bosilovich, M. G., Schubert, S. D.,  
915 Takacs, L., Kim, G.-K., Bloom, S., Chen, J., Collins, D., Conaty, A., da Silva, A., Gu, W., Joiner, J., Koster,  
916 R. D., Lucchesi, R., and Molod, A.: MERRA – NASA’s Modern-Era Retrospective Analysis for Research  
917 and Applications, *J. Clim.*, 24, 3624–3648, 2011.
- 918 Shindell, D. T., Chin, M., Dentener, F., Doherty, R. M., Faluvegi, G., Fiore, A. M., Hess, P., Koch, D. M.,  
919 MacKenzie, I. A., Sanderson, M. G., Schultz, M. G., Schulz, M., Stevenson, D. S., Teich, H., Textor, C.,  
920 Wild, O., Bergmann, D. J., Bey, I., Bian, H., Cuvelier, C., Duncan, B. N., Folberth, G., Horowitz, L. W.,  
921 Jonson, J., Kaminski, J. W., Marmer, E., Park, R., Pringle, K. J., Schroeder, S., Szopa, S., Takemura, T.,  
922 Zeng, G., Keating, T. J., and Zuber, A.: A multi-model assessment of pollution transport to the Arctic,  
923 *Atmos. Chem. Phys.*, 8, 5353-5372, doi:10.5194/acp-8-5353-2008, 2008.
- 924 Singh, P. and Bengtsson, L.: Hydrological sensitivity of a large Himalayan basin to climate change, *Hydrol. Process.*,  
925 18, 2363–2385, 2004.

- 926 Taylor, K. E., Stouffer, R. J., and Meehl, G. A.: An Overview of CMIP5 and the Experiment Design, *Bull. Am.*  
927 *Meteorol. Soc.*, 93, 485–498, doi:10.1175/BAMS-D-11-00094.1, 2012.
- 928 Wang, B., Bao, Q., Hoskins, B., Wu, G., and Liu, Y.: Tibetan Plateau warming and precipitation changes in East  
929 Asia, *Geophys. Res. Lett.*, 35, L14702, doi:10.1029/2008GL034330, 2008.
- 930 Wang, H., Easter, R. C., Rasch, P. J., Wang, M., Liu, X., Ghan, S. J., Qian, Y., Yoon, J.-H., Ma, P.-L., and Vinoj, V.:  
931 Sensitivity of remote aerosol distributions to representation of cloud-aerosol interactions in a global  
932 climate model, *Geosci. Model Dev.*, 6, 765–782, doi:10.5194/gmd-6-765-2013, 2013.
- 933 Wang, H., Rasch, P. J., Easter, R. C., Singh, B., Zhang, R., Ma, P. L., Qian, Y., and Beagley, N.: Using an explicit  
934 emission tagging method in global modeling of source-receptor relationships for black carbon in the Arctic:  
935 Variations, Sources and Transport pathways, *J. Geophys. Res.-Atmos.*, 119, 12888–12909, doi:  
936 10.1002/2014JD022297, 2014.
- 937 Wang, M., Xu, B., Cao, J., Tie, X., Wang, H., Zhang, R., Qian, Y., Rasch, P. J., Zhao, S., Wu, G., Zhao, H.,  
938 Joswiak, D. R., Li, J., and Xie, Y.: Carbonaceous aerosols recorded in a southeastern Tibetan glacier:  
939 analysis of temporal variations and model estimates of sources and radiative forcing, *Atmos. Chem. Phys.*,  
940 15, 1191-1204, doi:10.5194/acp-15-1191-2015, 2015.
- 941 Wang, X., S. J. Doherty, and J. Huang: Black carbon and other light-absorbing impurities in snow across Northern  
942 China, *J. Geophys. Res. Atmos.*, 118, 1471–1492, doi:10.1029/2012JD018291, 2013.
- 943 Warren, S. G. and Wiscombe, W. J.: A model for the spectral albedo of snow. II: Snow containing atmospheric  
944 aerosols, *J. Atmos. Sci.*, 37, 2734–2745, 1980.
- 945 Warren, S. G. and Wiscombe, W. J.: Dirty snow after nuclear war, *Nature*, 313, 469–470, 1985.
- 946 Wu, G., Liu, Y., He, B., Bao, Q., Duan, A., and Jin, F.-F.: Thermal controls on the Asian summer monsoon, *Sci.*  
947 *Rep.*, 2, 404, doi:10.1038/srep00404, 2012.
- 948 Xia, X. G., Zong, X. M., Cong, Z. Y., Chen, H. B., Kang, S. C., and Wang, P. C.: Baseline continental aerosol over  
949 the central Tibetan plateau and a case study of aerosol transport from South Asia, *Atmos. Environ.*, 45,  
950 7370–7378, 2011.
- 951 Xu, B., Cao, J., Hansen, J., Yao, T., Joswiak, D. R., Wang, N., Wu, G., Wang, M., Zhao, H., Yang, W., Liu, X., and  
952 He, J.: Black soot and the survival of Tibetan glaciers, *Proc. Natl. Acad. Sci. USA*, 106, 22114–22118,  
953 2009.
- 954 Xu, X., Lu C., Shi X., and Gao S.: World water tower: An atmospheric perspective, *Geophys. Res. Lett.*, 35, L20815,  
955 doi:10.1029/2008GL035867, 2008.
- 956 Yanai, M., Li, C., and Song, Z.: Seasonal heating of the Tibetan Plateau and its effects on the evolution of the Asian  
957 summer monsoon, *Journal of the Meteorological Society of Japan*, 70, 319–351, 1992.
- 958 Yao, T., Pu, J., Lu, A., Wang, Y., and Yu, W.: Recent glacial retreat and its impact on hydrological processes on the  
959 Tibetan Plateau, China, and surrounding regions, *Arct. Antarct. Alp. Res.*, 39(4), 642–650, 2007.
- 960 Yao, T., Thompson, L., Yang, W., Yu, W., Gao, Y., Guo, X., Yang, X., Duan, K., Zhao, H., Xu, B., Pu, J., Lu, A.,  
961 Xiang, Y., Kattel, D. B., and Joswiak, D.: Different glacier status with atmospheric circulations in Tibetan  
962 Plateau and surroundings, *Nat. Clim. Change*, 2, 663–667, doi:10.1038/nclimate1580, 2012.

- 963 Yasunari, T. J., Bonasoni, P., Laj, P., Fujita, K., Vuillermoz, E., Marinoni, A., Cristofanelli, P., Duchi, R., Tartari,  
964 G., and Lau, K.-M.: Estimated impact of black carbon deposition during premonsoon season from Nepal  
965 Climate Observatory – Pyramid data and snow albedo changes over Himalayan glaciers, *Atmos. Chem.*  
966 *Phys.*, 10, 6603–6615, doi:10.5194/acp-10-6603-2010, 2010.
- 967 Ye, D. and Gao, Y.: *Meteorology of the Qinghai-Xizang Plateau* (Chinese Science Press, Beijing, 1979).
- 968 Ye, D. and Wu G.: The role of the heat source of the Tibetan Plateau in the general circulation, *Meteorol. Atmos.*  
969 *Phys.*, 67, 181–198, doi:10.1007/BF01277509, 1998.
- 970 Ye, H., Zhang, R., Shi, J., Huang, J., Warren, S. G., and Fu, Q.: Black carbon in seasonal snow across northern  
971 Xinjiang in northwestern China, *Environ. Res. Lett.* 7, 044002, doi:10.1088/1748-9326/7/4/044002, 2012.
- 972 Yeh, T., Lo, S., and Chu P.: The wind structure and heat balance in the lower troposphere over Tibetan Plateau and  
973 its surrounding. *Acta Meteor. Sinica* 28, 108–121, 1957.
- 974 Zhang, R., Hegg, D. A., Huang, J., and Fu, Q.: Source attribution of insoluble light-absorbing particles in seasonal  
975 snow across northern China, *Atmos. Chem. Phys.*, 13, 6091-6099, doi:10.5194/acp-13-6091-2013, 2013.
- 976 Zhang, X. Y., Arimoto, R., Cao, J. J., An, Z. S., and Wang, D.: Atmospheric dust aerosol over the Tibetan Plateau, *J.*  
977 *Geophys. Res.*, 106(D16), 18 471–18 476, 2001.
- 978 Zhao, S., Ming, J., Xiao, C., Sun, W., and Qin, X.: A preliminary study on measurements of black carbon in the  
979 atmosphere of northwest Qilian Shan. *J. Environ. Sci.*, 24(1), 152-159, doi:10.1016/S1001-0742(11)60739-  
980 0, 2012.
- 981 Zhao, Z., Cao, J., Shen, Z., Xu, B., Chen, L- W. A., Ho, K., Han, Y., Zhu, C., and Liu, S.: Aerosol particles at a  
982 high-altitude site on the Southeast Tibetan Plateau, China: implications for pollution transport from South  
983 Asia, *J. Geophys. Res.-Atmos.*, 118, 11360–11375, doi:10.1002/jgrd.50599, 2013.

984

**Table 1.** List of sites for the observations of atmospheric BC surface concentrations used in this study to evaluate our model simulation.

Site	Latitude (°N)	Longitude (°E)	Elevation (m)		Sampling time	Observation method	Contributor
			observation	model			
<b>Muztagh Ata</b>	38.3	75.0	4500	3497	2003–2006	Thermal Optical Reflectance (TOR)	Cao et al., 2009
<b>Hanle</b>	32.8	79.0	4250	4862	2009–2010	Aethalometer	Babu et al., 2011
<b>Manora Peak</b>	29.4	79.5	1950	1409	2005–2008	Thermal Optical Transmittance (TOT)	Ram et al., 2010
<b>NCO-P</b>	28.0	86.8	5079	4604	2006–2008	Multi-angle absorption photometer (MAAP)	Marinoni et al., 2010
<b>Lulang</b>	29.5	94.4	3300	3370	2008–2009	TOR	Zhao et al., 2013
<b>NCOS</b>	30.8	91.0	4730	4956	2006–2007	TOR	Ming et al., 2010
<b>QSSGEE</b>	39.5	96.5	4214	2748	2009–2011	Aethalometer	Zhao et al., 2012

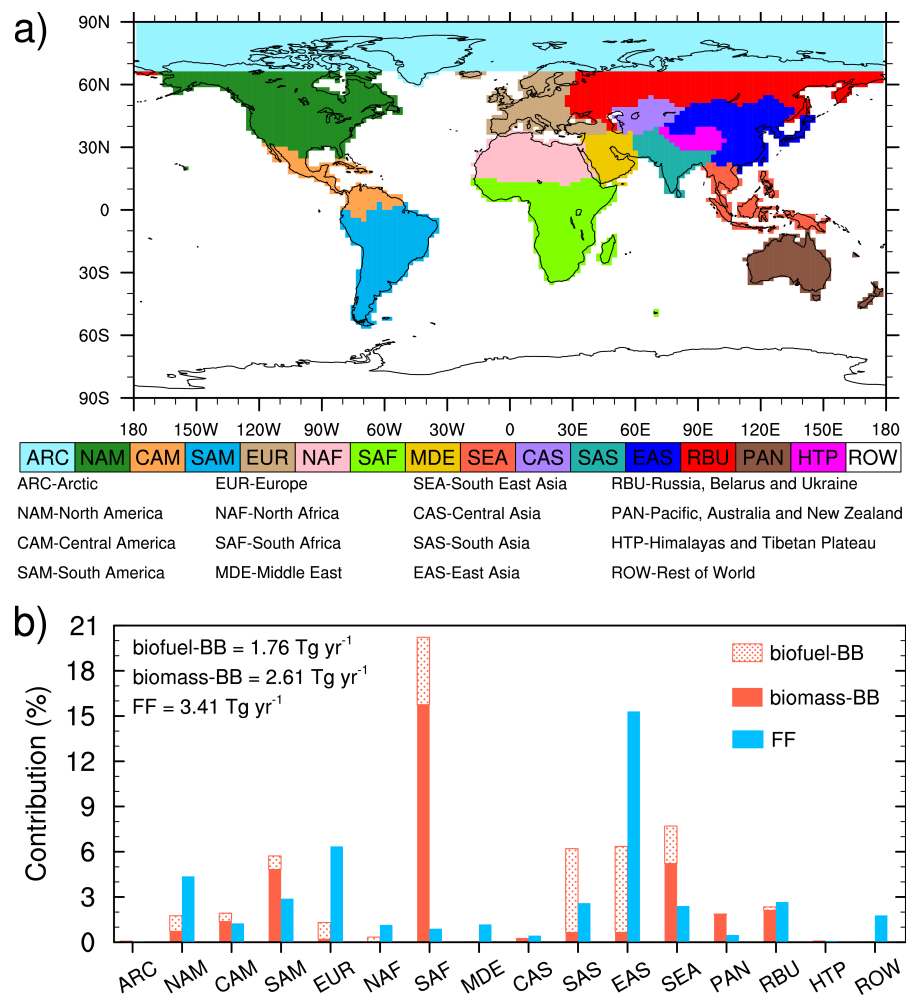


**Fig. 1.** (a) Tagged source regions and (b) the respective percentage contributions to global annual mean BC emissions from the individual source regions and sectors (including biofuel, biomass burning and fossil fuel). The global annual mean BC emission rate is  $7.78 \text{ Tg yr}^{-1}$ , which is divided up into the three sectors as indicated by the numbers at the upper-left corner.

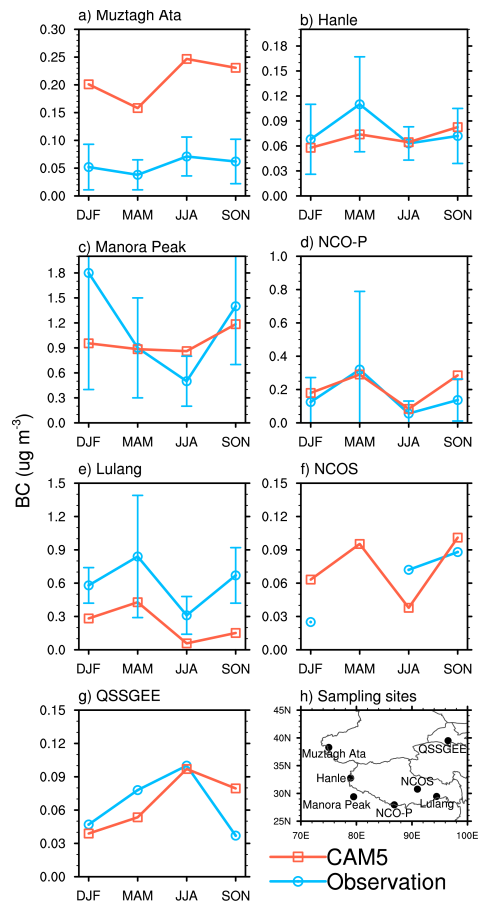


**Fig. 2.** Seasonal mean surface BC concentration ( $\mu\text{g m}^{-3}$ ) from observations (blue lines with error bars denoting SD) and CAM5 simulation (red lines) at the seven sampling sites listed in Table 1 and marked in map of panel h.

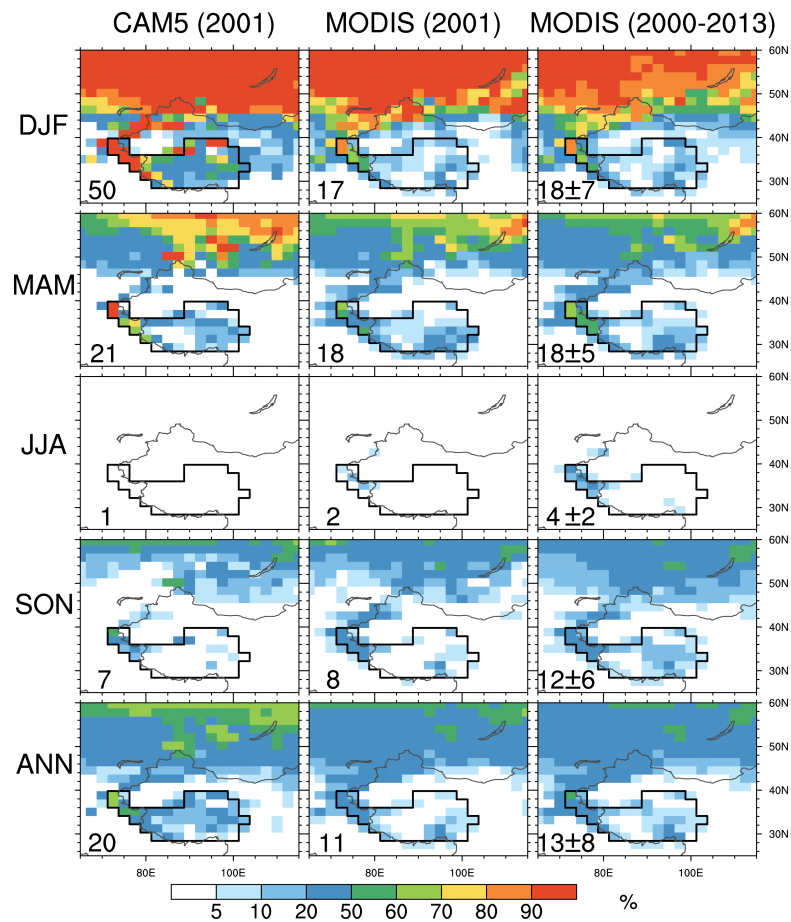


**Fig. 3.** Seasonal and annual mean snow cover fraction from CAM5 simulation for year 2001 (left), and MODIS retrieval for 2001 (middle) and 2000-2013 (right). The summer (JJA) in 2001 for both CAM5 and MODIS only includes July and August due to missing MODIS data in June. The number in the lower-left corner of each panel is the corresponding spatial mean SCF for the HTP region (which is marked with black outline), and for MODIS the standard deviation calculated from the MODIS multi-year means is also included.

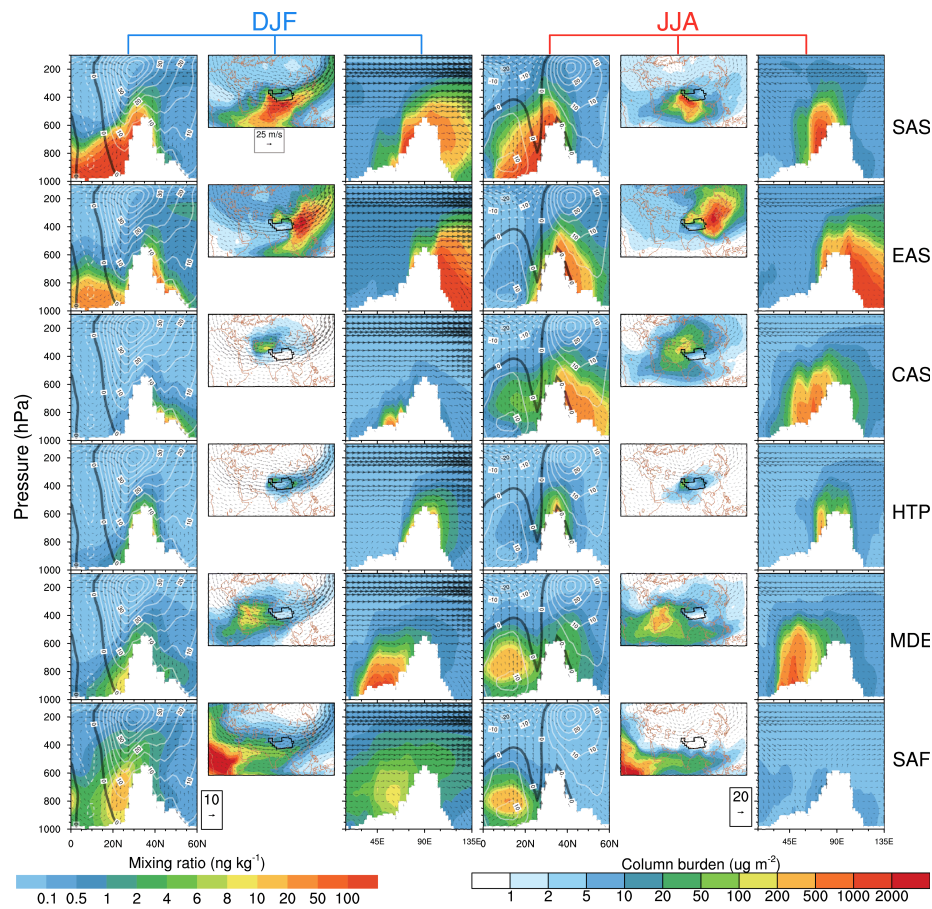


**Fig. 4.** The first column shows the latitude-height distributions of DJF BC mass mixing ratios (in  $\text{ng kg}^{-1}$ , colors) averaged over  $71.25\text{--}101.25^\circ\text{E}$ , originating from BB and FF sectors in the tagged source regions (corresponding to different rows); the white shaded area denotes topography, and the superimposed white contours at intervals of  $5 \text{ m s}^{-1}$  represent the westerly (solid) and easterly (dashed) DJF mean zonal winds along the cross-section with the thick solid black contour at  $0 \text{ m s}^{-1}$ ; the wind vectors (consisting of vertical velocity in units of  $-10^{-4} \text{ hPa s}^{-1}$  and meridional wind in  $\text{m s}^{-1}$ ) are represented by arrows. Colors in the second column denote spatial distribution of the DJF mean BC column burden (in  $\mu\text{g m}^{-2}$ ), originating from different source regions, and the arrows represent the DJF mean horizontal wind vectors at 500hPa; the HTP is marked with black outline. The third column is similar to the first column except that the quantities are on the longitude-height cross-section averaged over  $28\text{--}40^\circ\text{N}$ , and thus the horizontal component of the wind vectors is zonal wind ( $\text{m s}^{-1}$ ) instead. The fourth to sixth columns are the same as the first to third columns, respectively, but for JJA means instead.



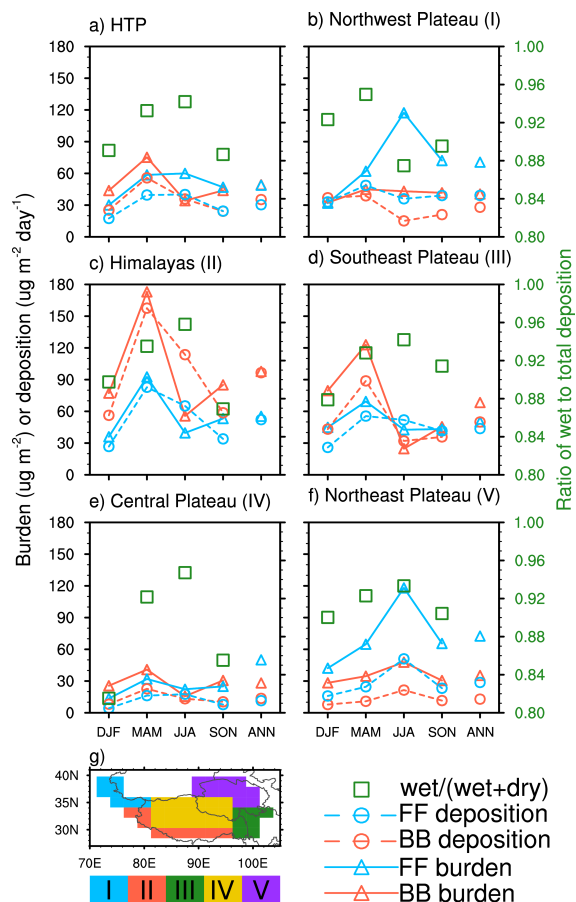


**Fig. 5.** Seasonal and annual mean BC column burden (solid lines and open triangles, in  $\mu\text{g m}^{-2}$ ) and deposition rate (dashed lines and open circles, in  $\mu\text{g m}^{-2} \text{ day}^{-1}$ ) over (a) the HTP, (b) Northwest Plateau, (c) Himalayas, (d) Southeast Plateau, (e) Central Plateau and (f) Northeast Plateau, emitted from BB (red color) and FF (blue color) source sectors. The green squares denote the ratio of wet to total BC deposition (using y-axis on the right) in four seasons over each receptor region. The geographical locations of five sub-regions of HTP are indicated in panel g.

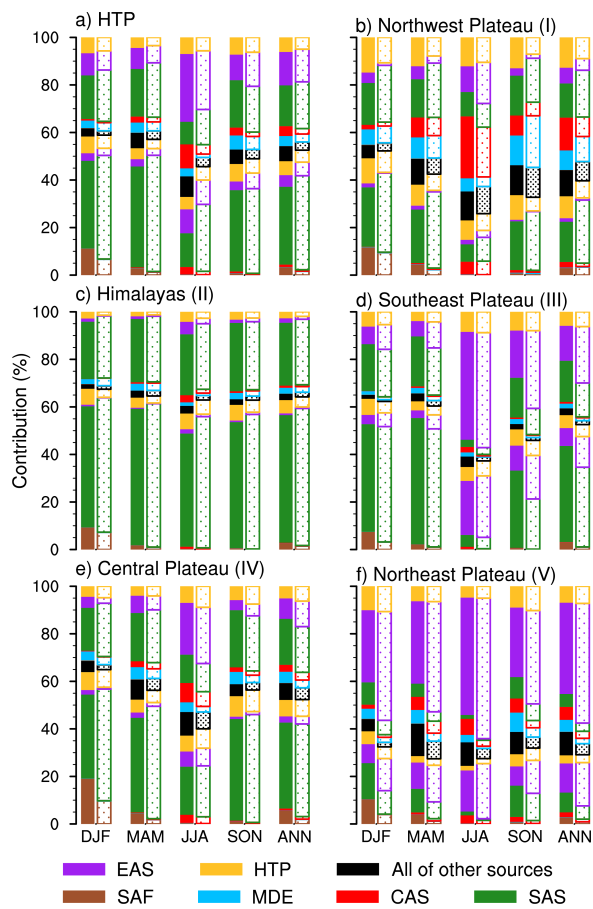


**Fig. 6.** Fractional contributions (measured by the lengths of color bars) to seasonal and annual mean BC column burden (solid pattern bars) and deposition (dotted pattern bars) over (a) the HTP, (b) Northwest Plateau, (c) Himalayas, (d) Southeast Plateau, (e) Central Plateau, and (f) Northeast Plateau, originating from six major tagged source regions (indicated by colors at the bottom) for BB (colors below the black bar) and FF (colors above the black color) emissions. The black bar in each column represents the contribution from all of the other tagged source regions and sectors.

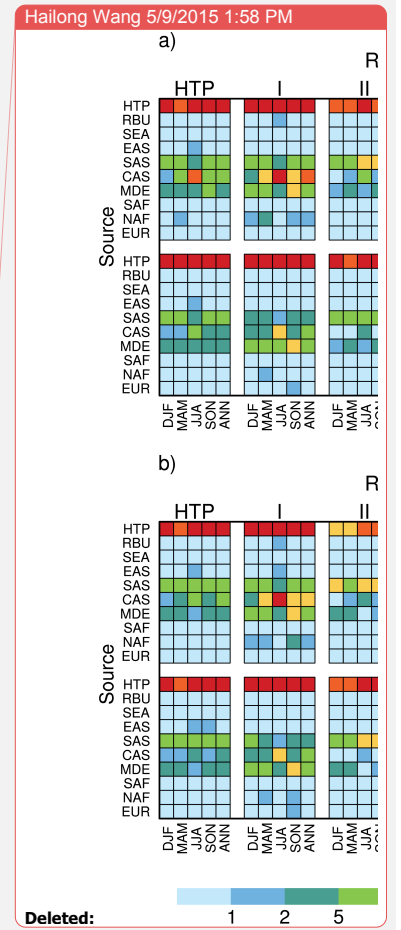
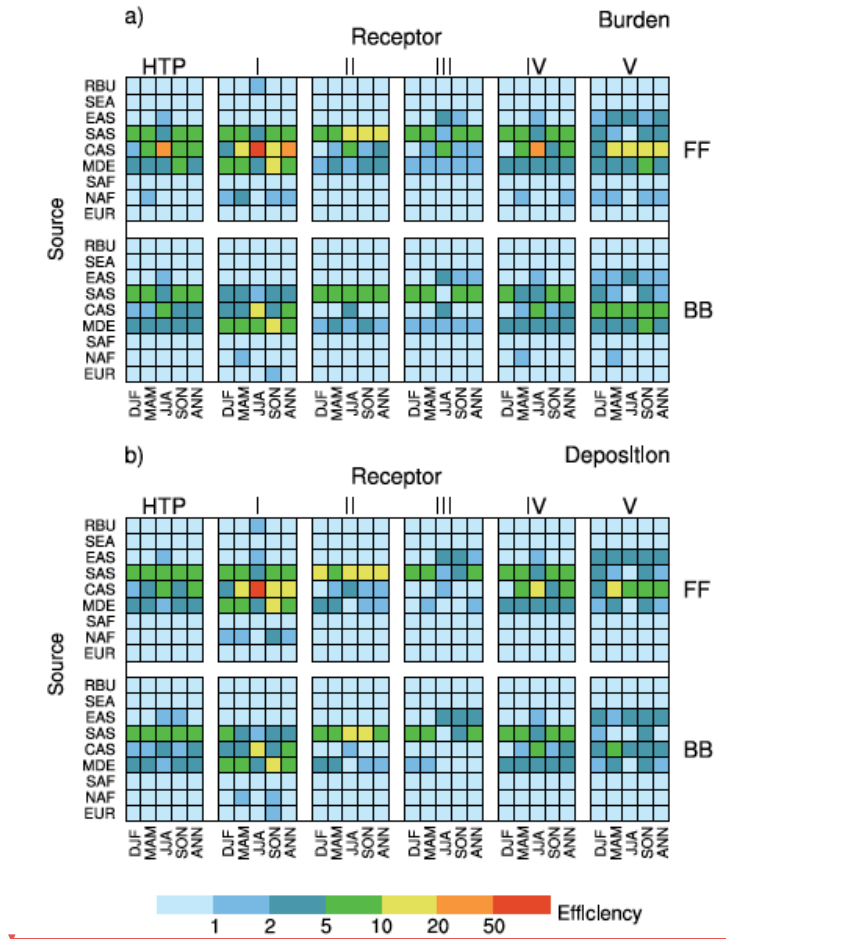


**Fig. 7.** Efficiency of FF (top) and BB (bottom) emissions from ten source regions (on the y-axis) in changing seasonal and annual mean (a) BC column burden and (b) deposition over the HTP and each of the five sub-regions: Northwest Plateau (I), Himalayas (II), Southeast Plateau (III), Central Plateau (IV) and Northeast Plateau (V).

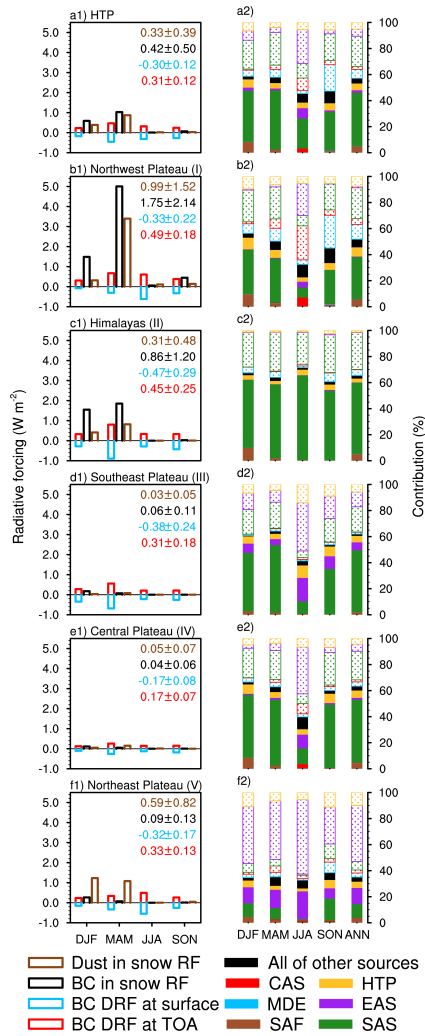


**Fig. 8.** Seasonal mean radiative forcing (left column) induced by the various BC effects (indicated by the color legend at the bottom) and dust-in-snow effect over (a1) the HTP, (b1) Northwest Plateau, (c1) Himalayas, (d1) Southeast Plateau, (e1) Central Plateau and (f1) Northeast Plateau. The corresponding annual mean forcings and one SD (for 12 monthly means) are shown in numbers on the top-right corner of each panel. The right column (a2-f2) panels represent source contribution to surface BC-in-snow radiative forcing over the corresponding receptors from tagged source regions (colors) and sectors (solid pattern bar and dotted pattern bar for BB and FF, respectively). The black bar in each column represents the contribution from all of the other tagged source regions and sectors.